Influenza virus evolution and defective genome formation are shaped by host genotype and sex

Rodrigo M. Costa[1*], Lehi Acosta-Alvarez[1], Kaili Curtis[1], Kort Zarbock[1], Justin Kelleher[1], Bhawika S. Lamichhane[2], Andrew L. Valesano[3], William J. Fitzsimmons[3], Adam S. Lauring[3], Jon Seger[1], Frederick R. Adler[1] & Wayne K. Potts[1]

[1]School of Biological Sciences, University of Utah, Salt Lake City, UT, USA

[2]Department of Neurology and Neurological Sciences, Stanford University School of Medicine, Stanford, CA, USA

[3]Department of Internal Medicine and Department of Microbiology and Immunology, University of Michigan, Ann Arbor, MI, USA.

*Corresponding author: rodrigomcosta@gmail.com

ABSTRACT

Host-specific factors, including genetic background and sex, shape viral adaptation and influence virulence, yet their interactions and quantitative effects remain poorly understood. Additionally, multiple infections, where a host is infected with viruses from more than one source, are hypothesized to enhance viral diversity and increase virulence, but their impact in vertebrate hosts remains largely unexplored.

We experimentally adapted influenza A virus (IAV) to male and female BALB/c and C57BL/6 mice under single and multiple infection conditions. Using a novel three-dimensional mapping approach, we identified genotype- and sex-specific selection hotspots that drive viral adaptation at multiple scales, from localized substitutions to broader structural changes. Our findings reveal that host genotype plays a dominant role in shaping viral evolution, with sex-dependent selection patterns observed in certain contexts. In BALB/c-adapted viruses, selection favored mutations at a specific site of a protein interface in females, whereas male-adapted lineages exhibited a more diffuse distribution of mutations across the same region. We further demonstrate that host genotype influences the formation of defective viral genomes (DVGs), with C57BL/6-adapted viruses accumulating significantly more and longer deletions, leading to reduced cytopathic effect and altered virulence trajectories.

Multiple infections accelerated viral adaptation, increasing replication and mortality in a host-dependent manner. Adaptation to BALB/c hosts selected for high-virulence variants that maintained pathogenicity across diverse host backgrounds, whereas C57BL/6-adapted viruses exhibited attenuated virulence in novel hosts. These findings highlight the role of host genotype and sex in shaping viral evolution, reveal a previously unrecognized host-specific effect on DVG formation, and provide insights into how multiple infections drive the emergence of virulence-associated variants.

INTRODUCTION

Emerging infectious disease can trigger pandemics such as the 1918 influenza A virus (IAV) pandemic, which caused over 50 million deaths, and the SARS-CoV-2 pandemic, responsible for over 10 million deaths worldwide since 2019. In both pandemics, the second wave resulted in higher mortality suggesting that, following a host switch, early pathogen evolution in immunologically naive populations favors mutations enhancing replication and shedding rather than antigenic escape[1–3]. Adaptation to naive mammalian hosts is primarily shaped by host genetic factors and innate immune responses, more so than evasion of adaptive immunity. This highlights the importance of investigating how host-specific innate immune responses influence virulence evolution.

Differences in immune responses across different host genotypes and sexes are well-documented. For instance, BALB/c and C57BL/6 mice exhibit distinct immune profiles that affect infection outcomes[4,5]. Similarly, female mammals typically mount stronger immune responses than males, leading to faster virus clearance but a higher risk of immunopathology. However, while males are more susceptible to infection, they experience less severe immune-mediated damage[6,7]. These differences likely play important roles in pathogen evolution, as host resistance and tolerance are thought to select for increased pathogen replication speed and virulence[8].

Studies on mammalian pathogens show that while adaptation to resistant host genotypes can increase virulence within those hosts, it may reduce pathogen fitness and virulence in novel hosts[9–11]. However, other studies suggest that adaptation to resistant genotypes can enhance virulence across all host types[12,13]. Similarly, theoretical models propose that, like resistant genotypes, the robust immune responses of females may drive the evolution of virulence-associated traits[8,14]. Yet, beyond limited experimental work in invertebrates and the discovery of a male-specific mutation in hepatitis B virus, the role of sex in virulence evolution remains largely unexplored[15–17]. This underscores the need for further studies to investigate not only the independent effects of host genotype and sex on pathogen evolutionary trajectories, but also their interactions, which are particularly understudied.

By exerting selective pressure on viral populations, immune responses usually reduce genetic diversity and virulence[18,19]. Purifying selection and genetic drift limit viral evolution, while narrow transmission bottlenecks further restrict the emergence of new variants [20,21]. In contrast, higher genetic diversity has been shown to enhance fitness and virulence in RNA viruses, particularly in novel host environments[22–24]. Thus, mechanisms that increase viral diversity, such as multiple infections, can mitigate the effects of bottlenecks and accelerate adaptation. Multiple infections are necessary for the antigenic shift responsible for IAV pandemics, but they can also generate virulent seasonal strains, such as the intra-subtype reassortant responsible for the severe 2017–2018 epidemic[25]. Despite accounting for an estimated 3% to 13% of IAV cases[26–29], research on the evolutionary effects of multiple infections is limited to theoretical models and invertebrate studies[30,31]. Experimental studies in vertebrate hosts are needed to understand how multiple infections shape viral adaptation and virulence.

In this study, we investigate how host genotype and sex shape viral evolution by adapting IAV to male and female BALB/c and C57BL/6 mice, revealing virulence-associated genotype- and sex-specific adaptations that rise to high frequency across multiple independent viral lineages. Additionally, we investigate the impact of increased viral diversity through different pooling treatments, which simulate multiple infections and influence virulence outcomes. Utilizing a novel three-dimensional structural mapping approach, we identify host-specific substitutional hotspots, including sex-based differences in the distribution of mutations across a protein interface. We discover that host genotype significantly influences the formation of defective viral genomes, which alter replication dynamics and immune interactions. Our findings provide new insights into the role of host genotype and sex in viral adaptation, with implications for understanding pathogen evolution in diverse populations.

RESULTS

The evolution of viral replication phenotypes is host-genotype dependent

To investigate how host genotype and sex affect the evolution of influenza A virus (IAV), we adapted the original H3N2 human isolate A/Hong Kong/1/68 (HK68) to both female and male BALB/cJ and C57BL/6J mice (hereafter referred to as BALBF, BALBM, BL6F, and BL6M viruses). We also aimed to assess the effect of multiple infections on viral adaptation and how it interacts with host background to influence virulence evolution. For this, we infected ten mice of each host type with HK68 and selected the four viruses with the highest lung titers in each group, designated as round 1 (R1) A, B, C, and D (Fig. 1A) . These four initial viruses served as the starting point for seven independent viral lineages in each host group. Viruses were passaged for 10 rounds of infection using three different strategies: single-host passages (1X), where viruses from R1 A, B, C, and D were passaged independently for 10 rounds; two-host

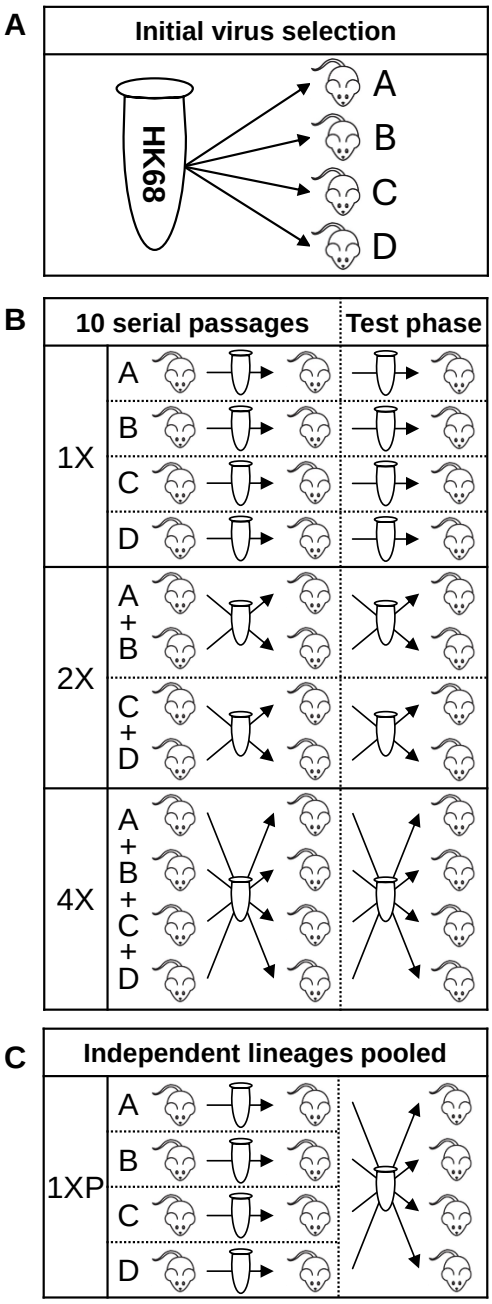

Fig. 1 – Experimental design. A) HK68 virus was used to infect ten mice of each host type. The 4 highest titer viruses in each host, deemed R1, were selected to start all passage lineages for that host. B) Passages were conducted for 10 rounds. 1X - single-host passages; 2X - two-host pooled passages; 4X - four-host pooled passages. C) 1XP lineages were comprised of the evolved 1X lineages pooled at the test phase only.

pooled passages (2X), where viruses from R1 A and B were pooled to create lineage AB, and viruses from R1 C and D were pooled to create lineage CD; and four-host pooled passages (4X), in which viruses from R1 A, B, C, and D were all pooled to create lineage ABCD (Fig. 1B). Each infection lasted 3 days, and this process was conducted for all four host groups, resulting in a total of 28 adapted viral lineages. This experimental design ensured a common origin for the lineages within each host group and allowed us to systematically assess the impact of host genotype, sex, and pooling on viral evolution.

First, we wanted to determine whether adaptation to distinct host backgrounds impacts viral fitness, using whole-lung viral load as the measure of viral replication. We quantified titers for all viral lineages through $TCID_{50}$ assays on lung homogenates collected at 3 days post infection. Adaptation to BALB/c mice significantly increased viral titers in both sexes (Fig. 2A), with adapted lineages exhibiting higher lung viral loads than the ancestral HK68 strain (BALBF: $U = 306$, $p < 0.001$; BALBM: $U = 312$, $p < 0.001$) (Fig 2A). However, C57BL/6 adaptation resulted in significantly reduced $TCID_{50}$ values compared to HK68 in males and did not lead to increased titers in females (BL6M: $U = 207$, $p = 0.004$; BL6F: $U = 169.5$, $p = 0.156$). These results suggest that viral replication is primarily affected by host genotype, with an additional, genotype-dependent effect of host sex.

To ensure that viral passages were successful, qualitative RT-PCR was performed each round to confirm the presence of virus in lung homogenates. By round 10, cycle threshold values for both BL6F and BL6M lineages were similar to those of BALB/c, indicating normal replication in C57BL/6 mice. Given that C57BL/6-adapted lineages had significantly reduced $TCID_{50}$ values compared to HK68, we hypothesized that C57BL/6 adaptation led to a loss of cytopathic effect in the MDCK cells used for titration, particularly in male-adapted virus. To test this, we performed standardized RT-qPCR on R10 samples from each evolved lineage to explore the relationship between viral RNA copy numbers and $TCID_{50}$ values.

Comparisons between host-adapted viruses revealed copy numbers were not significantly different (KW statistic = 3.7617, $p = 0.288$) (Fig. 2B). Furthermore, there was a strong positive correlation between $TCID_{50}$ and copy number in BALBF ($r_s = 0.893$, $p = 0.012$) and BL6F lineages ($r_s = 0.847$, $p = 0.016$), although BL6F titers were about an order of magnitude lower for the same copy number (Fig. 2C). BALBM lineages had a similar but not statistically significant relationship between titer and copy number ($r_s = 0.449$, $p = 0.312$). However, for BL6M, there was no correlation between $TCID_{50}$ and copy number ($r_s = -0.109$, $p = 0.816$), mostly due to $TCID_{50}$ values that were close to or below the limit of detection (10^3). The similarity between viral genome copy numbers across different hosts, along with the significant reduction in measured titers in C57BL/6 adapted lineages, indicates that adaptation to different host genotypes and sexes can strongly impact the cell culture infection phenotype and, consequently, traditional viral quantification methods.

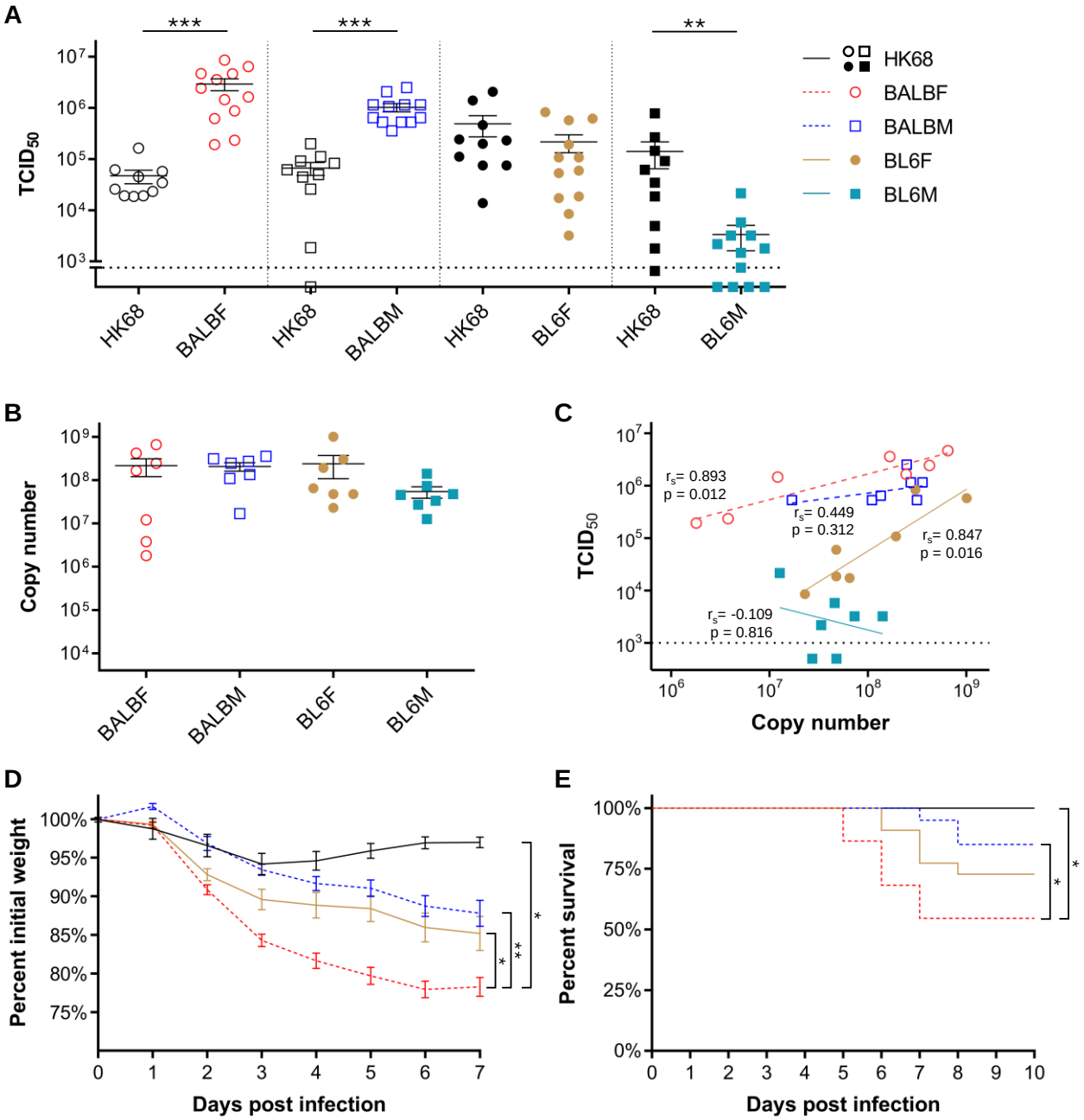

Fig. 2 – Titer and virulence measurements. A) Log10 TCID50 values for viral infections with ancestral HK68 (black) or mouse-adapted virus (colored). BALB/c females – open circles; BALB/c males – open squares; C57BL/6 females – solid circles; C57BL/6 males - solid squares. The bar at 10^3 $TCID_{50}$ represents the limit of detection. B) Log10 copy number per µL of viral RNA (M segment).
C) Correlation between log10 TCID50 and log10 vRNA copy number. Spearman's correlation coefficients (rs) were calculated for all independent lineages of each host-adapted virus. D) Weight loss (percent of initial weight) and E) survival curves for the ancestral and host-adapted viruses in the respective hosts. Black – Combined ancestral HK68 in all hosts; dashed red line – BALBF infections; dashed blue line – BALBM infections; solid brown line – BL6F infections. Weight loss was modeled until 7 days post infection. Error bars are SEM.

Host genetic background and sex alter virulence evolution trajectories

We next performed test phase infections to assess how adaptation to different hosts affects virulence, specifically in terms of weight loss and mortality. Evolved viral lineages were purified via overnight infections in cell culture (MOI = 0.1) to remove host associated factors present in lung homogenates, which were found to affect infection outcomes[32]. Comparing sequenced homogenates and cell-culture supernatants showed that this method did not significantly alter the vast majority of identified variants (r^2 = 0.953, p =< 0.001) (Fig. S1A) and provided better sequence quality (Fig. S1B). Purified samples were then titered for dose standardization in the test phase. Due to our inability to standardize dose based on $TCID_{50}$ for the BL6M lineages, test phase infections for assessment of weight loss and mortality were independently conducted for BALBF, BALBM and BL6F lineages.

To determine whether mouse-adapted viruses exhibited increased virulence compared to the ancestral HK68 strain, we tracked percent weight loss per day in infected mice and compared groups with linear mixed models (LMMs). Viral passaging enhanced virulence across all examined hosts, with greater weight loss observed in mice infected with the respective adapted viruses (Fig. 2D). Specifically, within each host, infection with the evolved virus resulted in more weight loss than infection with the ancestral virus. This effect was most pronounced in BALB/c female lineages, where BALBF virus caused 5.2 times more weight loss than the ancestral HK68 in that host (LMM; t = -2.868, p = 0.013). Similarly, BALBM and BL6F viruses caused mean daily weight losses in their hosts that were 5.0 and 3.3 times greater, respectively, than those induced by the unpassaged virus in each host. Although these increases suggest heightened virulence, they were not statistically significant (LMM; BALBM: t = -1.473, p = 0.164; BL6F: t = -1.384, p = 0.190), likely due to high variability in host response and thus higher variance in weight measurements within these groups.

We then compared the three evolved viruses to assess differences in virulence among host-adapted lineages in their respective hosts. BALBF virus was the most virulent, causing nearly twice the weight loss seen in BALBM (LMM; t = - 3.167, p = 0.005) and BL6F infections (LMM; t = -2.839, p = 0.011). In contrast, BALBM and BL6F infections caused comparable weight loss (LMM; t = 0.344, p = 0.735). These findings indicate that viral adaptation increased virulence in all hosts, with the most pronounced effect observe in BALB/c female-adapted lineages.

Adapted viruses caused enhanced mortality in infected mice compared to the ancestral HK68 virus, which caused no deaths (Fig. 2E). BALBF virus killed 45% of infected mice (Logrank; χ^2 = 5.975, p = 0.015), while BALBM and BL6F caused mortality in 15% (Logrank; χ^2 = 1.433, p = 0.231) and 27% (Logrank; χ^2 = 3.136, p = 0.077) of their hosts, respectively. Since the ancestral virus had no mortality, log-rank tests were used for these comparisons. For comparisons between evolved viruses, where mortality was present in all groups, we used Cox proportional hazards (CPH), which showed that BALBF virus induced significantly higher mortality than BALBM (CPH; hazard ratio [HR] = 4.2437, p = 0.028), but not BL6F virus (CPH; HR = 2.113, p = 0.148). These findings suggest that while viral passaging increases virulence and mortality, the extent of these

effects is host-dependent. Overall, these results underscore the critical role of host genotype and sex in shaping viral evolution.

Multiple infections during adaptation lead to increased replication and mortality

In addition to testing the effects of host genotype and sex on evolution, our experimental design allowed us to examine whether multiple infections influence viral evolution by comparing single-host passages (1X) with pooling at every round (2X and 4X). Pooling significantly influenced viral titers in BALB/C-adapted lineages (BALBF: KW statistic = 8, p = 0.018; BALBM: KW statistic = 6.979, p = 0.031), but not in C57BL/6-adapted viruses (BL6F: KW statistic = 2.989, p = 0.225; BL6M: KW statistic = 3.644, p = 0.162), likely due to the loss of cytopathic effect affecting real titers (Fig. S2A, D, G, J). Dunn's multiple comparison revealed significant differences between 1X and 4X in BALBF (z = 2.746, p = 0.009) and between 2X and 4X in BALBM (z = 2.640, p = 0.012). These results suggest that multiple infections during passage influence viral titers in specific genetic backgrounds, but the effect is context-dependent.

Pooling also influenced virulence. While multiple infections during passage slightly increased daily weight loss, high variance and small sample sizes limited the detection of significant differences using conservative LMMs (Fig. 3A). However, mortality increased consistently with the number of samples pooled during passage (Fig. 3B). 1X lineages caused a 12.5% mortality rate, compared with 31.8% for 2X (CPH; HR = 2.541, p = 0.177) and 50% for 4X (CPH; HR = 6.588, p = 0.006). Host-specific pooling effects were also analyzed (Fig. S2), revealing significantly increased mortality in mice infected with 4X BALBF virus (CPH; HR = 2.457, p = 0.014) but not in other hosts.

We hypothesized that a single multiple infection event with independently evolved lineages could enhance genetic diversity for selection within a host, facilitating fitness landscape traversal and maximizing virulence. To test this, we pooled all four 1X lineages for each host-adapted virus and infected the corresponding host type (Fig. 1C). Mice infected with the 1X pooled viruses (1XP) lost 45% more weight per day than mice infected with single lineages, though this increase was not significant (LMM; t = -1.232, p = 0.248). However, mortality was significantly higher, with 1XP killing 44.4% of mice, compared to the 12.5% mortality rate of the 1X lineages (CPH; HR = 4.629, p = 0.024),

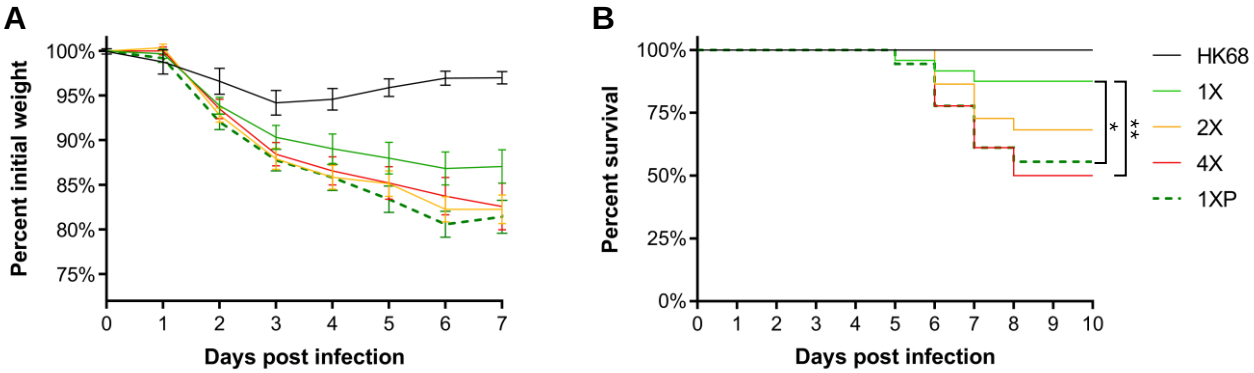

Fig. 3 – A) Weight loss and B) survival curves for the different passage treatments (1X - green, 2X - gold, 4X - red) and the single multiple infection event (1XP – dashed dark green) compared to ancestral HK68 (black).

approaching the overall mortality seen in the 4X treatment. This effect was strongly driven by BL6F virus, where mortality increased from 12.5% in 1X to 83% in 1XP (CPH; HR = 2.057, p = 0.040).

Despite significant mortality differences between pooling treatments and an overall trend of increasing virulence with the number of donor hosts, weight loss trajectories were more strongly defined by host type than by pooling treatments. These results suggest that while multiple IAV infections during or after serial passage enhance virulence, the effects of host genotype and sex exert a stronger influence on viral evolution.

A rolling sphere model reveals selection hotspots in three-dimensional space

Given that adaptation to different host genotypes and sexes resulted in distinct phenotypes for replication in cell culture and mammalian host virulence, we sought to determine if the observed phenotypic variation was underpinned by genetic differences. To this end, we conducted whole genome sequencing of the ancestral HK68 and the 28 independent mouse-adapted viral lineages at the final (R10) passage rounds. Of note, C57BL/6-adapted lineages exhibited higher sequencing coverage than BALB/c lineages, with BALB/c samples showing marked degradation, likely caused by heightened host RNase activity.

Genomic analysis revealed a diverse array of mutations at different frequencies, dispersed across viral lineages. All non-synonymous amino acid variants along with their respective frequencies are presented in Fig. S3 and Table S1. Several variants reached high frequency or even fixation in multiple lineages, suggesting positive selection. While shared variants were readily identifiable, we encountered instances where high frequency variants were either closely spaced or dispersed across the nucleotide sequence space. This observation suggested these 'hotspots' could indicate broad selective pressures acting on protein interfaces or entire domains. Initially, we employed a "rolling window" approach to detect genomic regions with elevated non-synonymous variant frequencies. However, this method failed to capture interactions between amino acids that, while distant in linear sequence space, were in proximity within the three-dimensional architecture of quaternary protein structures.

To address this, we devised a “rolling sphere” model that iteratively navigates along the protein chains, detecting significant increases in cumulative variant frequency within a designated radius of each amino acid (Video S1). The model was run on the entire dataset and then separately for viral lineages adapted to each host group, allowing the distinction between general mammalian/mouse adaptations and those unique to specific hosts. Two distinct sphere radii were employed in sequential runs. First, a 6 Ångström (Å) radius to detect single amino acid mutations at sufficiently high frequency across various lineages, as well as direct interactions between neighboring amino acids. This was followed by running a broader 12 Å radius to capture larger interfaces and identify potential allosteric effects. This strategy not only addresses challenges posed by the spatial complexity of proteins but also accommodates interactions within both homomeric and heteromeric oligomers, enhancing our understanding of host-specific evolutionary pressures on viral processes.

Host genotype and sex determine the emergence of virulence-associated variants

The rolling sphere model identified various residues and hotspots under selection, demonstrating its power to capture patterns of adaptation at several scales. Table 1 shows significant hotspots (99.9th quantile) and includes the average variant frequency within each host group, as well as the general impact on viral replication and/or virulence of each variant, if previously described in the literature. Additionally, to improve the understanding of the spatial distribution of variants identified by the rolling sphere model and their potential impact on protein function, we mapped the mean variant frequencies for each host onto three-dimensional protein structures.

At the residue scale, the rolling sphere model revealed several notable host-specific adaptations associated with increased virulence and replication. In the hemagglutinin (HA) protein (Fig. 4), two previously described mutations within the receptor-binding pocket, G218W and G218E, were present at high frequency almost exclusively in BALB/c females, achieving fixation or near-fixation (>90%) in 5 out of 7 BALBF lineages. Consistent with this observation, our review of the literature revealed that these mutations were exclusively reported in studies utilizing female BALB/c or CD-1 mice[33–36], emphasizing that sex- and genotype-specific selective pressures drive the emergence of the G218 variants. These mutations have been shown to elevate the fusion pH for HA through alterations in the receptor-binding pocket[37], likely facilitating viral fusion earlier during endosome maturation. In contrast, the HA mutation N165D was found at high frequency across all other host groups but was only detected at a very low frequency (1.2%) in the single BALBF lineage lacking a G218 mutation,

Protein	Variant	Freq BALBF	Freq BALBM	Freq BL6F	Freq BL6M	Effect	Refs
HA	N165D	0.002	**0.263**	0.137	0.054	Increased virulence	38,39
HA	G218W/E	**0.705**	0.002	-	-	Increased replication but not virulence. Increases fusion pH	37,40
NS1	G183E/R	**0.567**	0.131	0.016	0.074	Interface-disrupting mutations can reduce virulence	42,43
PA	M21I	0.157	0.129	-	0.142	Increased polymerase activity	40
PA	T97I	0.225	0.138	-	0.107	Increased polymerase activity	40
PB2	K482R	**0.349**	-	0.143	-	Increased polymerase activity, virulence and replication	40
PB2	D701N	0.014	0.014	0.129	**0.425**	Increased polymerase activity, virulence and replication	40
PB2	D740N	0.160	**0.332**	0.143	-	Increased polymerase activity, virulence and replication	40

Table 1 – Positively selected variants. Variant frequencies under each host are the mean of seven independent lineages. Bolded frequencies denote variants significant in the specific host at 6 Å.

possibly indicating they are mutually exclusive. N165D removes an N-glycosylation site near the head region of HA, and has been associated with increased weight loss and mortality in previous studies[38,39].

In the polymerase (Fig. 5), three positively selected mutations were identified in the polymerase basic 2 (PB2) subunit, K482R, D701N, and D740N, all previously linked with increased polymerase activity and virulence in mammals[40,41]. K482R is situated within the midlink domain of PB2 and is crucial for nuclear-cytoplasmic shuttling of the polymerase complex. This variant emerged solely in female hosts of both genotypes, suggesting a sex-specific adaptation. On the other hand, D701N and D740N exhibited marked genotype-specific trends. D701N became fixed or nearly fixed in four C57BL/6-adapted lineages (three males and one female), while D740N was found predominantly in BALB/c hosts (six BALB/c lineages versus a single BL6F lineage).

Interestingly, we identified a synonymous mutation in the M2 protein, Y52Y (TAT→TAC), which, although present in the ancestral virus at about 8.4% frequency, rose to fixation or near-fixation in 23 out of 28 viral lineages across all four hosts. Neuraminidase (NA), nucleoprotein (NP), matrix protein 1 (M1), and matrix protein 2 (M2) did not show significant nonsynonymous positive selection signals and are therefore not shown or discussed. Additionally, the smaller proteins—PA-X, NEP (nuclear export protein), and PB1-F2—were not included in the rolling sphere analysis or 3D models due to the absence of suitable Protein Data Bank (PDB) structures.

These findings collectively demonstrate the capacity of the rolling sphere model to detect critical residues under positive selection across different host groups. Notably, variants linked to high fitness and virulence were found within specific host genotype-sex combinations, suggesting that unique host backgrounds may play a crucial role in the emergence of general mammalian adaptations within a population.

Spatial analysis provides insights into host-dependent selection at multiple scales

The use of two distinct rolling sphere sizes allowed us to gain deeper insights into how structural and functional contexts shape viral adaptation. At the interface scale, the model identified a hotspot within the effector domain (ED) of the NS1 protein (Fig. 6), specifically at the glycine dimerization motif of the helix-helix interface[44]. The site G183, detected as a significant hotspot using the 6 Å rolling sphere radius in BALBF but not in BALBM, harbored the variants G183E/R, which alter a key glycine residue involved in NS1 ED-ED dimerization. However, applying the model with the 12 Å radius revealed that the same interface is a hotspot in BALBM virus, as multiple sites, including G183, exhibited high mutation rates into charged residues. In each lineage, only one helix variant was present at high frequency, suggesting that any single mutation along the interface may be sufficient to inhibit dimerization in male hosts, whereas BALBF lineages exhibited targeted mutations at G183.

The detection of this hotspot in the NS1 of BALB/c-adapted viruses suggests genotype-specific selection for the disruption of ED-ED dimerization, essential for antagonizing the OAS/RNase L pathway, among other functions[45]. Disruption by these mutations may lead to elevated RNase activity, contributing to the viral RNA degradation observed

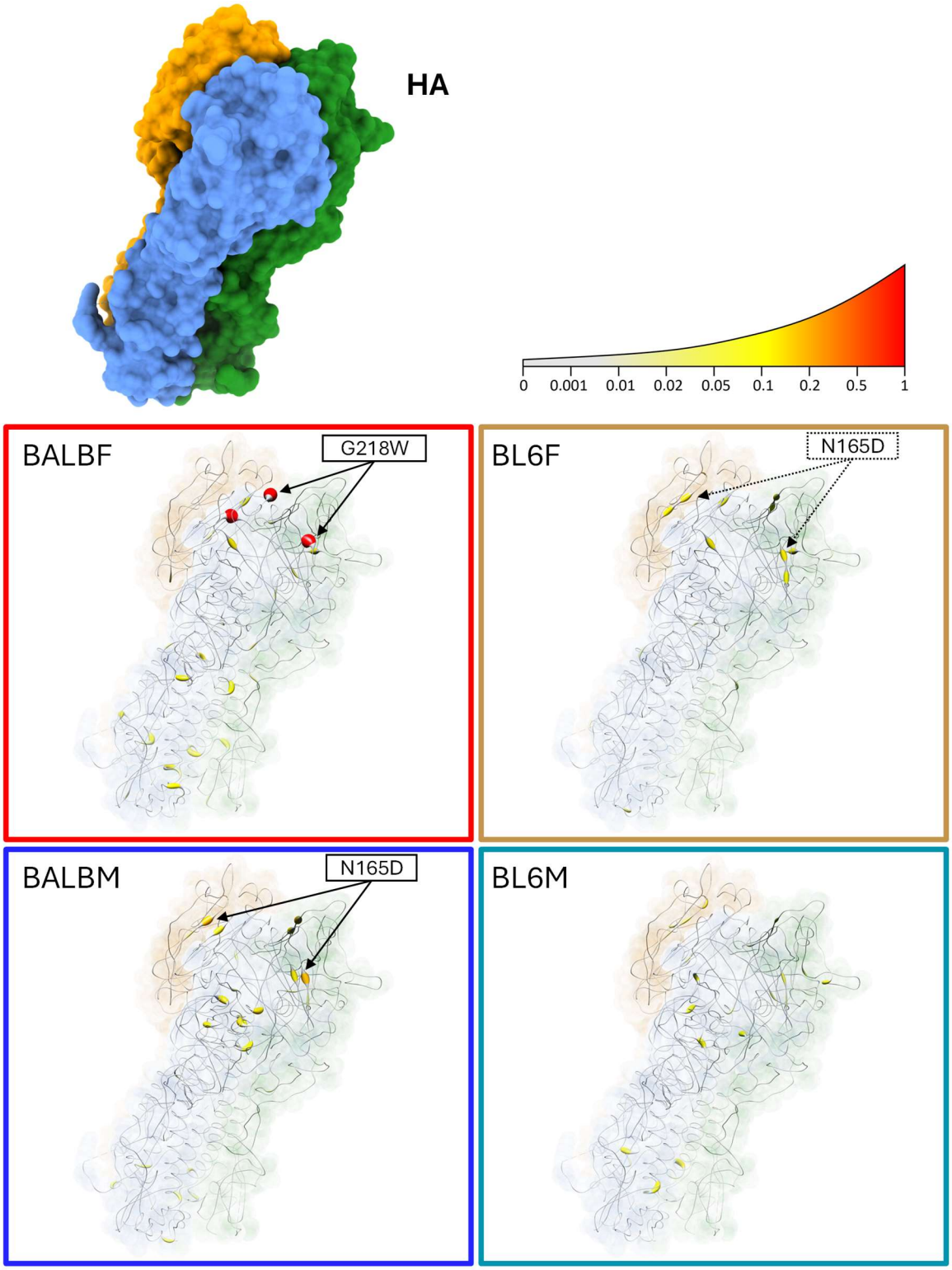

Fig. 4 – Three-dimensional protein models for the hemagglutinin homotrimer (PDB: 7QA4). For each host, the mean frequency of each variant across the seven independent lineages is represented by the color intensity and thickness of the simplified amino acid chains within the structure of each protein. Variants of interest are identified as the nexus of significant hotspots within a host type (solid lines), or at high frequency in at least one lineage, but not significant (dotted lines).

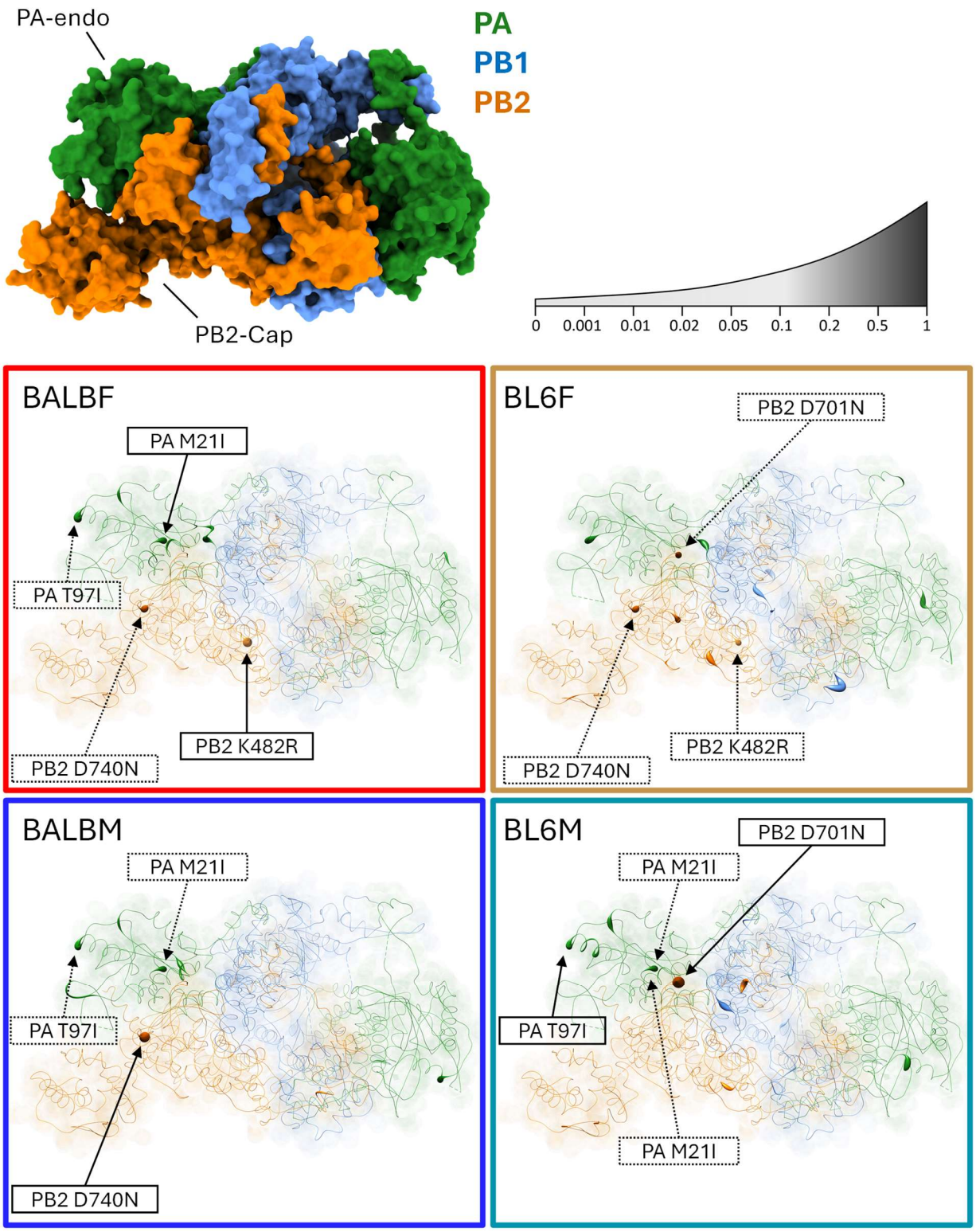

Fig. 5 – Three-dimensional protein models for the polymerase heterotrimer. (PDB: 6QNW). For each host, the mean frequency of each variant across the seven independent lineages is represented by the thickness of the simplified amino acid chains within the protein structure. Variants of interest are identified as the nexus of significant hotspots within a host type (solid lines),or at high frequency in at least one lineage, but not significant (dotted lines).

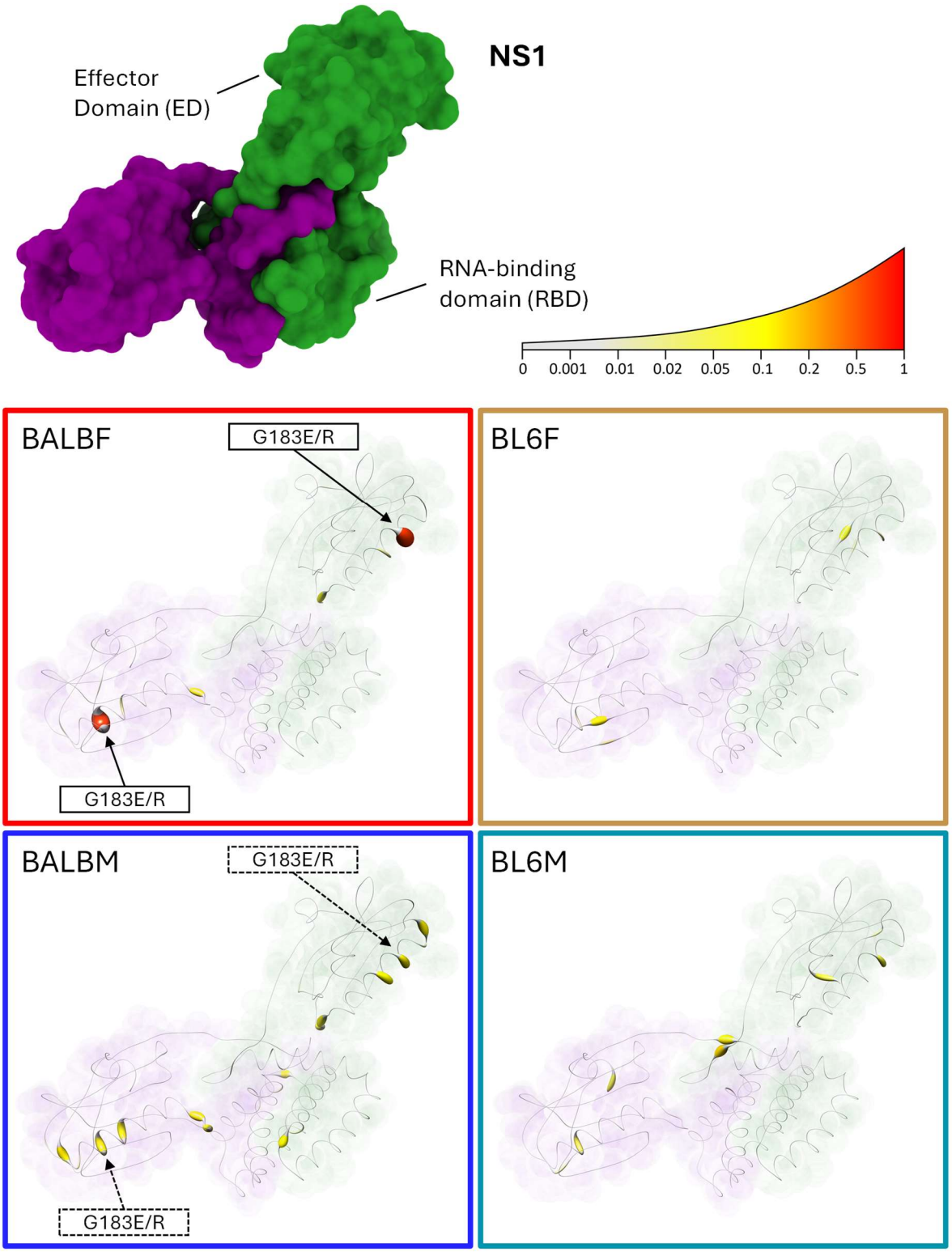

Fig. 6 – Three-dimensional protein model for the NS1 homodimer (PDB: 4OPH). For each host, the mean variant frequency of the seven independent lineages is represented by the color intensity and thickness of the simplified amino acid chains within the structure of each protein. Variants of interest are identified as the nexus of significant hotspots within a host type at 6 Å (solid lines) or 12 Å (dashed lines).

in BALB/c samples, and potentially resulting in increased inflammation and virulence. More importantly, these genotype-specific adaptations were shaped by host sex: female adaptation led to targeted selection at a specific residue, whereas male adaptation resulted in a more dispersed mutational landscape across the ED-ED dimerization interface. To our knowledge, this sex-dependent mode of viral adaptation at the protein interface level has not been previously documented, and suggests that host sex plays a critical role in shaping selective pressures on viral proteins.

At a domain level, the rolling sphere model identified significant hotspots within the Polymerase Acidic endonuclease (PA-endo) domain, responsible for cleaving host mRNAs and cap-snatching. Notably, two high-frequency variants, M21I and T97I, were detected by the model and observed across multiple hosts. These and numerous other low-frequency variants scattered throughout this domain and neighboring PB2 residues contributed to its identification as major hotspot at the 12 Å radius in BALB/c-adapted viruses. The surprisingly high mutational tolerance of the PA-endo domain implies it may be a suboptimal target for antivirals. In fact, we identified three low-frequency mutations at residue I38 (I38M/T/V), two of which have been shown to confer resistance to the antiviral baloxavir marboxil[46]. This shows that 3D variant frequency scanning can provide critical insights into the mutability of key protein domains and inform rational drug design strategies targeting less variable regions, thereby reducing the likelihood of drug resistance evolution.

As our results indicated host-specific differences in selective pressures across structural scales, we sought to examine how adaptation influenced broader evolutionary trajectories. To this end, we performed principal component analysis (PCA) on the cumulative variant frequencies within the 6 Å and 12 Å radii centered at each amino acid site of each evolved lineage, and included the ancestral HK68 strain as a baseline reference (Fig. 7). The PCA revealed distinct clustering of viral lineages based on host genotype, with BALB/c-adapted lineages diverging further from HK68 than C57BL/6-adapted lineages. Furthermore, while lineages adapted to C57BL/6 mice of both sexes clustered closely, BALBF and BALBM lineages showed greater separation at 6 Å, but less so at 12 Å. This suggests that sex-specific adaptation plays a more pronounced role in BALB/c hosts, and that some of the observed variation is reduced at a larger scale, reflecting the differences in variant distribution across the NS1 ED helix-helix interface. Overall, by integrating spatial and functional dimensions, the rolling sphere model shows host-specific selection at broader structural and functional scales beyond single-site substitutions. This multi-scale approach reveals how genotype and sex shape interact to shape viral evolution, particularly in driving the emergence of virulence-associated variants.

Host genotype and sex influence defective viral genome formation

C57BL/6-adapted lineages did not exhibit shared substitutions or hotspots that could explain their distinctive cell culture phenotype, prompting us to investigate alternative causes for the observed discrepancy between viral titers and genome copy numbers in these hosts. A known contributor to reduced tissue culture infectivity is the accumulation of defective viral genomes (DVGs). Once thought to be laboratory artifacts causing reduced IAV infectivity after serial passages in eggs[47–49], these truncated viral genomes

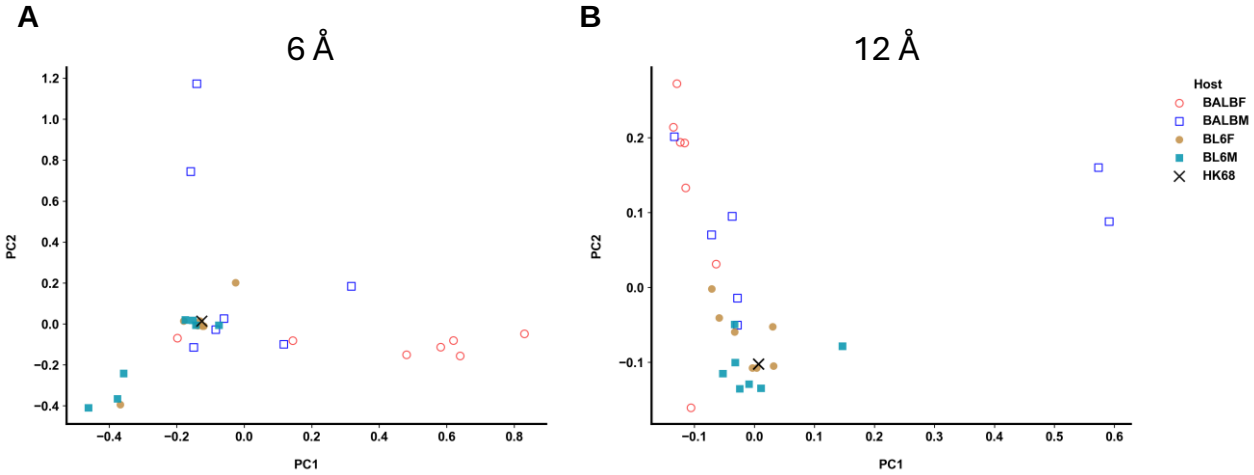

Fig. 7 – PCAs for the sum of cumulative frequencies at each site for 6 Å (A) and 12 Å (B). Ancestral HK68 is marked as a black X.

are now recognized as naturally occurring elements that can be packaged into virions, interfering with viral replication and significantly affecting viral fitness and persistence[50,51]. Recent studies confirm that DVGs are present in human infections, modulating the immune response and reducing virulence, which highlights their important role *in vivo*[52–54].

To assess whether DVGs were responsible for reduced infectivity, we searched for deletions of 3 or more nucleotides across viral genomes obtained from R10 lung homogenates. Consistent with previous studies on influenza DVGs, deletions were primarily found at both ends of the polymerase segments (PB1, PB2, PA), a hallmark of DVG formation[55]. The frequency, location and length of deletions for the polymerase segments and HA are shown in Figure 8 (A–D). DVG distribution varied significantly across host groups, with differences in the mean number of deletions (KW statistic = 40.53, $p < 0.001$) and deletion length (KW statistic = 11.23, $p = 0.011$), although deletion frequency was not significantly different (KW statistic = 3.77, $p = 0.287$).

Host genotype was a key factor influencing DVG formation, with C57BL/6 viruses displaying more numerous ($U = 414.5$, $p < 0.001$) and longer deletions ($U = 1156.5$, $p = 0.021$) than BALB/c viruses. Additionally, male-adapted viruses had longer deletions than female-adapted viruses ($U = 1524$, $p = 0.029$), indicating that host sex may also affect DVG formation. This aligns with the observation that BL6M lineages had lower $TCID_{50}$ values than BL6F lineages, supporting the hypothesis that DVGs are responsible for the reduced cytopathic effect. These findings, summarized in Table S2, highlight the substantial influence of host genotype and sex on DVG formation. The increased number and length of deletions in C57BL/6, particularly in male lineages, likely contribute to a higher proportion of defective viral genomes, which may explain the breakdown in correlation between $TCID_{50}$ and copy number in these viral lineages. Notably, titers across all hosts were strongly inversely correlated with the number of deletions ($r_s = -0.628$, $p < 0.001$) and their length ($r_s = -0.567$, $p = 0.005$) (Fig. 8E–G).

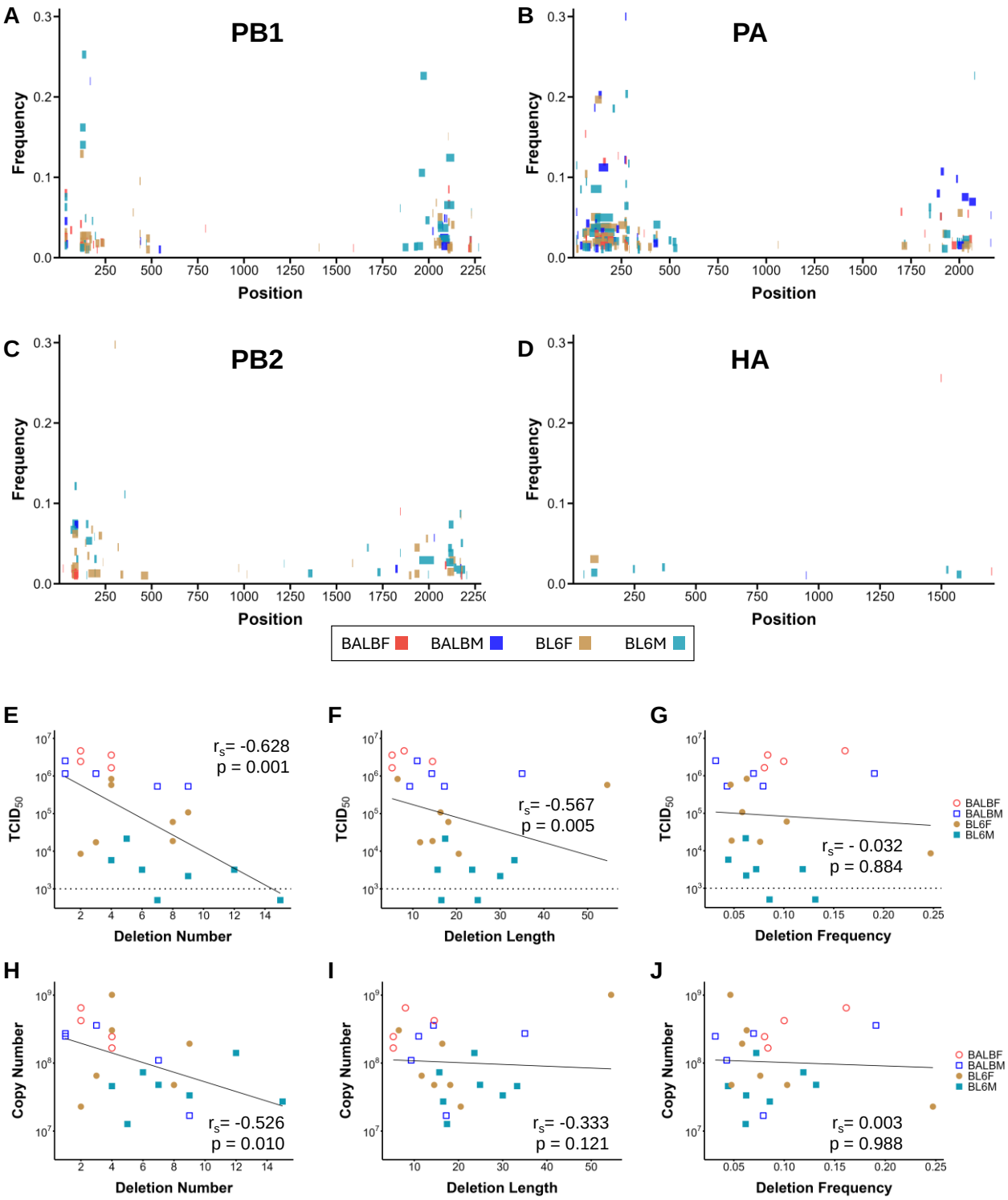

Fig. 8 – Defective viral genome differences by host. A-D) Genomic position (x-axis), Frequency (y-axis) and length (width) of deletion variants for the polymerase segments and hemagglutinin. All lineages within each host are combined. E-J) Spearman's correlations between TCID50 and deletion number (E), deletion length (F) and deletion frequency (G), and correlations between genome copy number and deletion number (H), deletion length (I) and deletion frequency (J). Samples with mean polymerase coverage below 100 reads were excluded.

However, copy number also correlated negatively with the number of deletions (r_s = -0.526, p = 0.010) (Fig. 8H–J), indicating that DVGs not only disrupt cytopathic effect but may also impair replication. Overall, these findings provide the first demonstration of host-induced differences in DVG formation in mammalian hosts, highlighting that viral adaptation can occur not only through selection of genetic variants but also by exploiting host-specific immune mechanisms that balance persistence and virulence.

Viral adaptation to specific host genotypes increases virulence in all hosts

Having established that adaptation to different host genotypes leads to viral populations that are not only genetically divergent but also exhibit varying levels of viral diversity and DVG content, we sought to evaluate how host-adapted viruses perform in their original (familiar) versus a novel (unfamiliar) host environment. To this end, we infected female C57BL/6 mice with the BALBF lineages and female BALB/c mice with the BL6F lineages to assess weight loss and mortality outcomes compared to familiar virus infections. The BALBF virus caused significantly more weight loss (LMM; t = 2.388, p = 0.049) and mortality (CPH; HR = 3.198, p = 0.001) than BL6F virus (Fig. 9A, B). Furthermore, while BALBF virus caused similar mortality in both hosts (Logrank; χ^2 = 1.390, p = 0.238), BL6F virus exhibited significantly lower mortality in BALB/c mice (Logrank; χ^2 = 4.364, p = 0.037). This suggests that while C57BL/6-adapted virus lost virulence in a novel host, the BALB/c-adapted virus retained higher virulence across host genotypes, regardless of familiarity.

Overall, for both familiar and unfamiliar viruses, C57BL/6 females exhibited slightly higher mortality than BALB/c female mice, though this was not significant (CPH; HR = 1.407, p = 0.159). This outcome is consistent with the heightened variability in C57BL/6 immune responses, which can either mitigate infection effectively or exacerbate immunopathology and increase mortality. This bimodal response, evident in Fig. 9A, explains the higher variance and the lack of statistical significance in some comparisons, despite clear differences in mean weight loss. In contrast, the BALB/c mice showed more uniform responses, resulting in lower variance and more consistent outcomes across infections. These findings underscore the interplay of host-specific immune dynamics with viral virulence across familiar and novel environments.

Neither weight loss nor survival of unfamiliar hosts were significantly affected by pooling during passage compared to 1X infections (Fig. 9C, D). Furthermore, while pooled 1X virus (1XP) was the most virulent infection treatment in novel hosts, causing 59% more weight loss and nearly double the mortality of single 1X lineages, these increases were not significant (LMM; t = -1.413, p = 0.206; CPH; HR = 3.013, p = 0.062). Nevertheless, 1XP emerged as the most virulent treatment when considering both familiar and unfamiliar infections across all host types. Survival analysis revealed a significant increase in mortality, with 1XP infections making mice three times more likely to die than those infected with the single 1X lineages (HR = 3.043, p = 0.011). This increase in mortality exceeded that of 2X (HR = 1.73, p = 0.247) and 4X (HR = 2.783, p = 0.021). Together, these results suggest that single multiple-infection events with independently evolved lineages may provide a broader sample of variants conferring high fitness and virulence, resulting in the most pronounced effects on host survival.

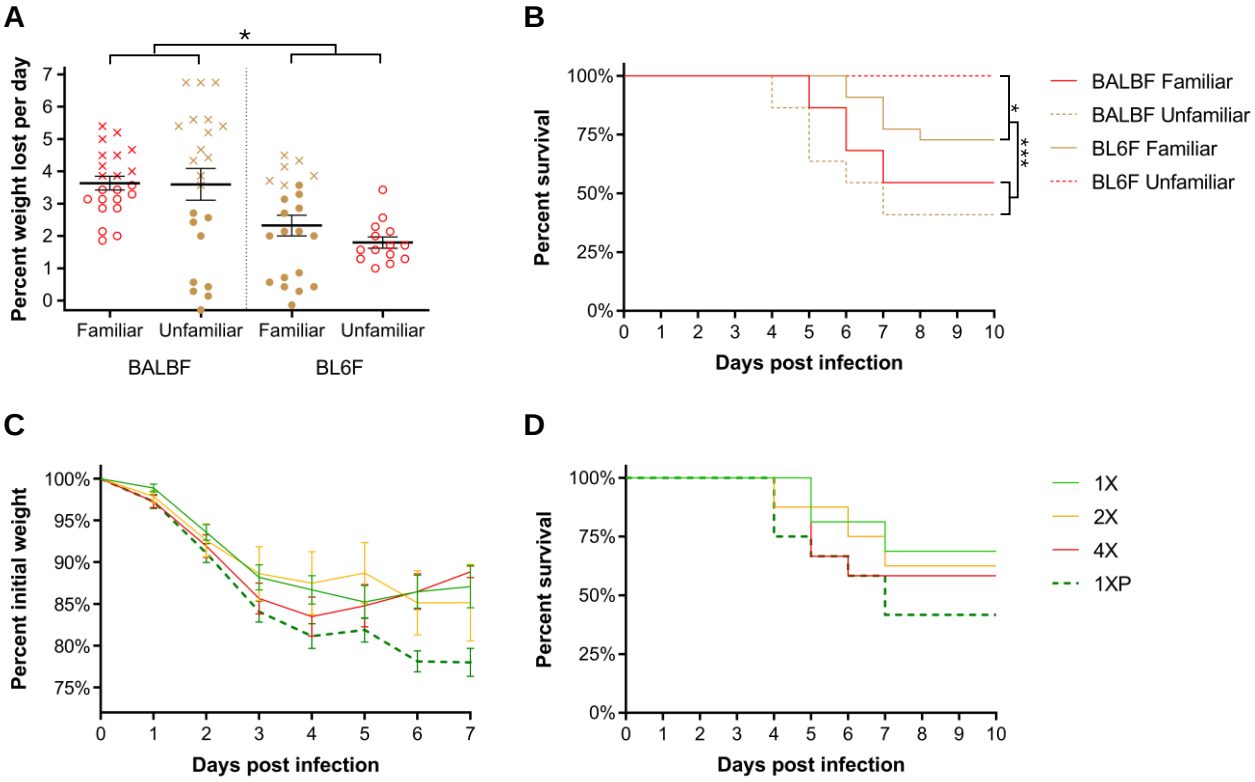

Fig. 9 – A) Weight loss (mean percent weight lost per day) and B) survival curves for familiar and unfamiliar host infections with BALBF and BL6F virus. BALB/c females - open red circles; C57BL/6 females – solid brown circles. Mice that died are represented as crosses. C) Weight loss and D) survival curves for the different passage treatments in unfamiliar hosts.

Combined, these data demonstrate that while multiple infections affect virulence, and variation in individual host immune responses influence whether viral infection is mitigated early, the primary determinant of a virus's overall virulence and mortality is its evolutionary history. Specific host genotypes drive the selection of high-virulence variants, such as the BALB/c female-specific G218W/E, and this virulence can persist across different host strains, regardless of the specific host environment and mode of infection.

DISCUSSION

The vast diversity of host genotypes in natural environments poses a significant challenge for comprehensively studying how interactions between host and viral diversity shape pathogen evolution. Experimental evolution offers a controlled framework to address this complexity. Our lab has previously used this approach to demonstrate that adaptation of the Friend virus complex to specific host genotypes or different MHC backgrounds leads to tradeoffs in fitness and virulence when infecting unfamiliar hosts[10,11,56,57]. Here, building on these findings, we sought to understand how selective pressures imposed by different combinations of host genotype and sex modulate influenza A virus evolution. Additionally, we explored whether emulating

multiple infections by pooling viral samples during or after serial passage impacts viral evolution and virulence.

Experimental adaptation resulted in two distinct evolutionary trajectories: while the ancestral HK68 virus exhibited lower fitness and virulence in BALB/c mice than in C57BL/6, adaptation in BALB/c selected for variants that increased virulence across both genotypes, supporting the hypothesis that resistant hosts drive selection for heightened pathogen virulence. In contrast, adaptation in C57BL/6 mice primarily selected for reduced cytopathic effect. Although these phenotypic differences were clear, traditional viral genomic analysis methods were insufficient to capture the full scope of molecular patterns underlying these adaptations. To address the complexity of host-pathogen interactions beyond linear sequence data, we developed a rolling sphere model to scan three-dimensional protein structures for increases in cumulative variant frequencies, supported by 3D model visualization.

Mapping mutations onto protein structures for functional interpretation is a common practice, particularly in cancer research, where several tools have been developed to predict the impact of single nucleotide polymorphisms on protein function. However, most tools primarily assist in visual detection of substitutional hotspots and do not automatically identify regions of increased activity[58,59]. While tools like VIVID have successfully applied a sliding-window approach to identify hotspots on individual proteins[59,60], our model stands out by automatically detecting hotspots across the entire pathogen genome, as long as PDB-derived residue distance matrices are provided.

The rolling sphere model revealed that genotype and sex significantly influence the substitutional landscapes of influenza A virus across different host backgrounds. Notably, selection did not act uniformly across viral proteins or regions. For instance, while PB2 mutations such as PB2 K482R, D701N, and D740N displayed genotype- and sex-specific selection patterns, the effects of sex were particularly pronounced in BALB/c-adapted viruses. The exclusive fixation of G218W/E mutations in the HA receptor-binding pocket among BALB/c female lineages suggests a unique selective pressure favoring accelerated viral entry. Similarly, in the NS1 ED domain, BALB/c female-adapted viruses accumulated mutations disrupting dimerization at a single site within the ED-ED binding interface, whereas male-adapted viruses exhibited mutations at multiple residues across the interface. This contrast between targeted (female) and broad (male) selection highlights how different host environments can shape viral adaptation at a structural level. To our knowledge this phenomenon has not previously been described.

The ability of certain hosts to select for virulence-associated viral variants that increase pathogenicity across diverse genetic backgrounds underscores the critical role of host-specific immune pressures in shaping pathogen evolution. Viruses exhibit high mutation rates, and every possible single nucleotide mutation presumably occurs multiple times during an infection. While genomes carrying new variants may have increased fitness and the potential to outcompete their precursors over time, the transmission of nonsynonymous mutations is often constrained by purifying selection and genetic drift imposed by bottlenecks within and between hosts[20,21]. Consequently, hosts where specific high-virulence variants gain a significant fitness advantage—such as the

BALB/c female-specific HA G218W/E—may be crucial for these variants to reach frequencies sufficient for successful transmission between hosts. Understanding intra-host competition between variants will be pivotal for determining whether high-virulence variants confer increased fitness across diverse hosts and whether specific host genotypes are crucial for their emergence and persistence. If host-specific viral mutations persist over time as they circulate through genetically diverse populations, infections in certain host backgrounds may trigger punctuated evolutionary bursts with broader implications for viral fitness and transmissibility.

Beyond the selection of single nucleotide variants, our study reveals that host genotype—and, to a lesser extent, sex—significantly influences defective viral genome formation, adding another layer to the molecular battle between hosts and viruses. While cell culture studies have suggested that host factors may influence DVG production[61,62], our findings provide the first *in vivo* evidence of host-genotype-specific DVG formation. Deletion profiling revealed C57BL/6-adapted viral populations accumulated more numerous and longer deletions, which are associated with DVG formation. Research shows DVG-rich cells trigger antiviral immunity through interferon signaling while inhibiting apoptosis, enabling persistent infections[63]. The resulting reduction in virus-induced apoptosis would explain the attenuated cytopathic effect observed in C57BL/6-adapted viruses. Although we did not directly test DVG transmissibility into BALB/c, this mechanism may also explain the reduced virulence of C57BL/6-adapted lineages.

DVG accumulation can reduce tissue damage while extending infection duration and shedding, potentially creating a trade-off between reduced virulence and transmissibility. Furthermore, by reducing the effective viral population size, DVG accumulation likely enhance purifying selection for competent genomes, limiting the transmission of low-frequency variants and ultimately constraining viral adaptability across host environments. Understanding DVG transmission dynamics and how they affect viral evolution in natural populations could significantly improve strategies for controlling viral diseases. Additionally, identifying host-specific cellular mechanisms that drive DVG formation may guide antiviral approaches that promote DVG production, boosting immune responses while limiting virulence.

This study represents one of the first experimental investigations of multiple infections by an RNA virus in a vertebrate host. No positively selected variants were unique to any pooling treatment, suggesting that competition or cooperation between genomes did not significantly alter evolutionary trajectories. Instead multiple infections could accelerate sequence space exploration and increase virulence and mortality, both during adaptation and in single multiple infection events. The increased diversity generated by multiple infections may help overcome transmission bottlenecks induced by heightened immune responses and DVG formation, as seen in C57BL/6 mice, which were particularly affected by one-time multiple infections. Single multiple-infection events can enhance the virulence of contributing viral lineages, possibly through broader variant sampling or synergistic interactions among virulence-associated variants. These findings provide new insights into the evolutionary effects of multiple infections in vertebrates, especially in overcoming host-specific selective pressures.

In conclusion, our study demonstrates the profound impact of host genotype and sex-specific selection pressures on IAV evolution, emphasizing how intraspecies genetic diversity drives the emergence of virulence-associated variants. Our findings on viral adaptation dynamics—including the formation of DVGs and the influence of multiple infections—improve our understanding of how pathogens evolve in naive host populations, where transmission and replication take precedence over immune evasion. Work to elucidate host-specific mechanisms that facilitate the emergence of variants that increase virulence across host populations will inform epidemiological models and strategies to control the prevalence of infectious diseases.

METHODS

Mice

Infections were conducted on 7–24-week-old, age-matched C57BL/6J and BALB/cJ mice of both sexes, sourced from The Jackson Laboratory or bred in-house from Jackson Laboratory ancestry. Mice were acclimated for at least three days, provided food and water ad libitum, and singly housed for at least 24 hours prior to infection. A total of 686 experimental animal infections were conducted. All procedures were in accordance with University of Utah IACUC guidelines.

Viral rescue, propagation, purification and quantification

Influenza strain A/Hong Kong/1/1968 (HK68) was provided by Dr. Earl Brown (University of Ottawa) in the form of 8 plasmids, each containing an influenza segment. Viral rescue was performed by Dr. Matthew Angel and Dr. Jonathan Yewdell (NIH/NIAID, Bethesda, MD). Rescue of HK68 was performed as previously described with minor modifications[64]. Briefly, Lipofectamine 2000 (Invitrogen) and DNA were mixed at a ratio of 1 µL to 1 µg, respectively, and incubated for 30 minutes at room temperature. Opti-MEM (Gibco-BRL, Carlsbad, CA) was added to a total volume of 1 mL, and the transfection mixture added to a co-culture of MDCK/293T cells. Six hours post-transfection, the mixture was removed and replaced with 1 mL of Opti-MEM. At 24 hours post-transfection, 2 mL of Opti-MEM containing TPCK-trypsin (1 µg/ml) (Worthington, Lakewood, NJ) was added. At 3 days post-transfection, supernatant was harvested and inoculated into the allantoic cavity of 10-day-old SPF embryonated chicken eggs. At 48 hours post-inoculation, virus-containing allantoic fluid was harvested and stored at -80 ºC.

Viral titers were measured using standard $TCID_{50}$ assays in MDCK cells and calculated using the Reed-Muench method[65,66]. For intermediate passages, presence of virus in samples was determined by extracting RNA (Quick-RNA Miniprep, Zymo Research) and performing quantitative reverse transcription polymerase chain reaction (RT-qPCR) with the Verso 1-step RT-qPCR Kit (Thermo Fisher) using primers specific for the M segment of IAV[67].

Before test phases, evolved lineages were purified using a custom cell-culture method. Briefly, 6-well plates with confluent MDCK cells were inoculated with 400 µL of viral growth medium containing the post-passage lung homogenates (MOI = 0.1). After a 60 minute adsorption, lung-derived medium was washed off, replaced with new viral growth medium and incubated overnight at 37 ºC. After this incubation, medium was aspirated into a 2mL microtube, centrifuged for 5 minutes at 300 × g, 4 ºC, and the supernatant collected, mixed, aliquoted, and stored at -80 ºC.

MDCK cell maintenance medium was comprised of DMEM with high glucose, L-glutamine and sodium pyruvate (Genesee Scientific); 10% FBS, heat-inactivated (Gibco); 1% Penicillin-Streptomycin (Sigma-Aldrich, St. Louis, MO).

Viral growth medium was DMEM as above; 2.5% BSA (Fisher Scientific); 2.5% HEPES (Fisher Scientific); 1% Pen-Strep; 2 µg/mL TPCK-trypsin.

Viral passage and collection

Passages were performed using a slightly modified standard protocol[68]. Each passage was conducted using 20 µL intranasal inoculations in mice under isoflurane anesthesia. After 3 days mice were sacrificed and lungs extracted into a 2 mL microtube, homogenized with a rotor-stator homogenizer (Dremel) and brought up to a volume of 1 mL using PBS. Homogenates were centrifuged and supernatant collected, mixed, aliquoted, and stored at -80 ºC.

To measure virulence, mouse weights were recorded daily every 24 hours (±2h), and mice reaching 75% of their initial weight were euthanized for humane considerations. For test phases, weights were recorded for 10 days or until mice reached the weight threshold or showed prominent signs of distress.

All passages and test phases had animals balanced by litter, age and origin (ordered from The Jackson Laboratory or bred in our facility), to avoid any potential bias across treatments. All test phase mice received standardized doses of 4000 $TCID_{50}$ per inoculate.

Viral titer and virulence statistics

Viral titers were assessed using two distinct nonparametric approaches to account for non-normality and unequal variance that could not be addressed with transformation. For each host group, a Wilcoxon-Mann-Whitney test compared combined passage treatment titers (1X, 2X, 4X) against stock virus. Passage treatments were compared by Kruskal-Wallis tests, followed by Dunn's multiple comparison test (dunn.test[69]). For evaluation of association between viral copy number and $TCID_{50}$, we employed Spearman's rank correlation to accommodate non-linear relationships without assuming data normality.

Test-phase virulence was assessed using linear mixed models (LMMs) to predict body weight as a percentage of initial weight. The models included fixed effects for time (day postinfection), passage status (Passaged or Unpassaged), and host group (BALBF, BALBM, BL6F), as well as their interactions. Observations were nested within mouse ID and further nested within viral lineage to reflect the hierarchical structure of the data. Given LMMs' assumption of linearity, the analysis was limited to the first 7 days post-infection, as recovery in surviving mice leads to restored body weight. Independent analyses were conducted for different pooling treatments (1X, 2X, 4X, 1XP) and for familiar versus unfamiliar infections. For these analyses, host of adaptation was included as a fixed effect where appropriate. All LMMs were fitted using the lme4[70] package in R[71], with degrees of freedom estimated via Satterthwaite approximation (lmerTest[72]). Model selection was guided by corrected Akaike's Information Criterion (AICc) using the MuMIn package[73].

Differential mortality was assessed using Cox proportional hazards models with similar structures to the body weight analyses. For pairwise comparisons where the Cox proportional hazards model failed to converge due to an absence of mortality, log-rank tests were performed instead. Both tests done using the R survival package[74].

Sequencing

Viral RNA was extracted using the Purelink Pro 96 Viral RNA/DNA Purification Kit (Thermo Fisher) with automated processing on the EpMotion system, followed by elution in 100 µL of RNase-free water. RNA integrity was confirmed via multiplex RT-PCR using SuperScript III One-Step RT-PCR System with Platinum Taq High Fidelity DNA Polymerase (Thermo Fisher), amplifying all eight influenza A virus gene segments. PCR products were purified using Agencourt AMPure XP magnetic beads and verified via agarose gel electrophoresis.

Library preparation was conducted using the Illumina Nextera DNA Flex Library Prep Kit, followed by size selection and quantitation. Indexed libraries were pooled, and qRT-PCR was used to determine viral genome copy number prior to sequencing.

Reads were processed as described previously[20]. Briefly, adapters were removed using cutadapt, and reads were aligned to the HK68 reference genome with bowtie2. Duplicates were marked and removed using Picard and samtools, and variants were called using deepSNV. Filtering criteria included a p-value < 0.05, Phred quality score >35, mapping quality (MapQ) >30, and read positions between 40 and 200. Samples with low sequencing coverage were excluded from further analysis. All sample WGS data used in this manuscript can be accessed in BioProject PRJNA1228145.

Rolling sphere model

Selection hotspots were identified using a three-dimensional rolling window-style approach that calculates the sum of weighted variant frequencies within two defined radii (6 and 12 Å) around each residue in protein structures. The 6 Å radius captured local substitutions and direct residue interactions, while the 12 Å radius identified broader mutational clusters and potential allosteric effects. The model was applied separately to all viral lineages (all hosts combined), genotype groups (BALB/c, BL6), sex groups (males, females), and individual host groups (BALBF, BALBM, BL6F, BL6M) to identify selection patterns at multiple levels.

To determine significance, 20 randomizations were performed, recalculating variant sums at each site for all hosts combined. Sites exceeding the maximum randomized value were considered significant hotspots. Sites containing more than 67% of the summed frequencies within a sphere were designated as the nexus of a hotspot and used to distinguish whether selection targeted single amino acids or broader structural regions. From the sites identified using all host data, we conducted post hoc model iterations to identify mutations that were significant at the genotype, sex or individual host level. Those detected at high frequency in both individual host groups were classified as genotype- or sex-specific accordingly, while those present in only one host type were considered host-specific.

3D modeling and distance matrices

UCSF Chimera v1.16[75] and ChimeraX v1.9[76] were used for 3D visualization of molecular structures. B-factors in the protein data bank (PDB) files were replaced with the mean mutation frequency of all independently evolved lineages in each host group. Distance matrices for the rolling sphere were generated using the PDBparser module

from the Bio.PDB library in Python to compute pairwise distances between residue centroids. The PDBs used for visualization and/or distance matrix generation were: HA - 7QA4 (3D model) and 4WE4 (distance matrix); NS1 - 4OPH; NP - 6J1U; PB1/PB2/PA - 6QNW; NA - 7U4E; M1 - 6Z5J; and M2 - 2RLF.

Defective viral genome analyses

Genomic deletions were analyzed using conservative cutoffs. Samples with average coverage below 100 reads across the polymerase segments were excluded. Only deletions with a frequency of at least 3% and a minimum length of 3 nucleotides were included in the analysis. The average number of deletions, average deletion length and average deletion frequency per sample were calculated for each host group. Differences between groups were assessed using a Kruskal-Wallis test, followed by Dunn's multiple comparison test (dunn.test) for significant pairwise differences. For comparisons involving host genotype and host sex, Wilcoxon-Mann-Whitney tests were performed. Relationships between deletions and $TCID_{50}$ or copy number were assessed using Spearman's correlations. All plots were generated with R package ggplot2.

ACKNOWLEDGEMENTS

The authors thank Dr. Earl Brown (University of Ottawa) for providing the HK68 viral plasmids, Dr. Matthew Angel and Dr. Jonathan Yewdell (NIH/NIAID) for rescuing the virus and Dr. Jody Rosenblatt (King's College, London) for the MDCK cells. We thank Dr. James Ruff, Dr. Douglas Cornwall and Dr. Joseph Cauceglia for their contributions to the study's design and statistical analysis.

W.K.P. and F.R.A. were supported by the National Institutes of Health grant R01GM109500. R.M.C. was partly supported by the John H. Weis Memorial Graduate Fellowship. K.C. and K.Z. were supported by the Undergraduate Research Opportunities Program (UROP) at the University of Utah. A.S.L. was supported by a Burroughs Wellcome Fund Investigator in the Pathogenesis of Infectious Diseases award.

AUTHOR CONTRIBUTIONS

Conceptualization and experimental design: R.M.C., J.S., F.R.A. and W.K.P.; manuscript writing: R.M.C.; editing and revisions: R.M.C., B.S.L., A.S.L., J.S., F.R.A. and W.K.P.; viral passage, purification, processing and data collection: R.M.C., L.A.-A., K.C., K.Z. and J.K.; sequence analysis and statistical analyses: R.M.C., J.S. and F.R.A.; rolling sphere model development and implementation: R.M.C. and F.R.A.; Data visualization and figure preparation: R.M.C. and B.S.L.; Library preparation and viral sequencing: R.M.C, A.L.V., W.J.F., and A.S.L.

DECLARATION OF INTERESTS

The authors declare no competing interests.

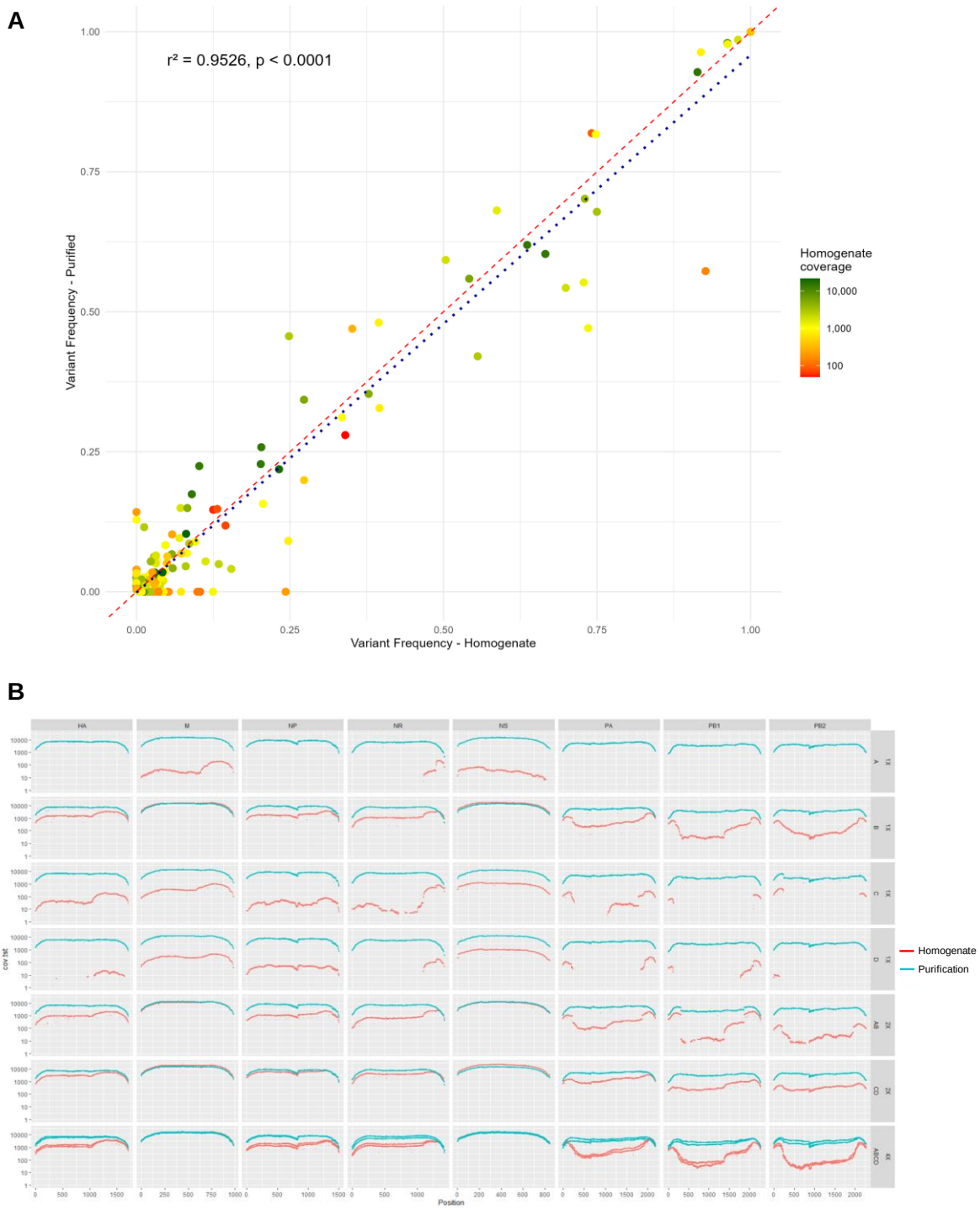

Fig. S1 – A) Comparison of variant frequencies in homogenates and purified samples. Each point represents a single variant, with the x-axis showing the frequency in homogenate samples and the y-axis showing the frequency in the respective purified samples. The color of each point indicates the coverage at that variant, (red = low coverage, green = high coverage). The red line represents the line of perfect concordance (y = x), indicating identical frequencies between the two datasets. The blue dotted line is the linear regression line, showing the observed relationship between the two sample sets ($r^2 = 0.9526$, $p < 0.0001$). B) Coverage maps for homogenates (red) and purified (blue) samples. Each column represents a genomic segment and each row is a viral lineage.

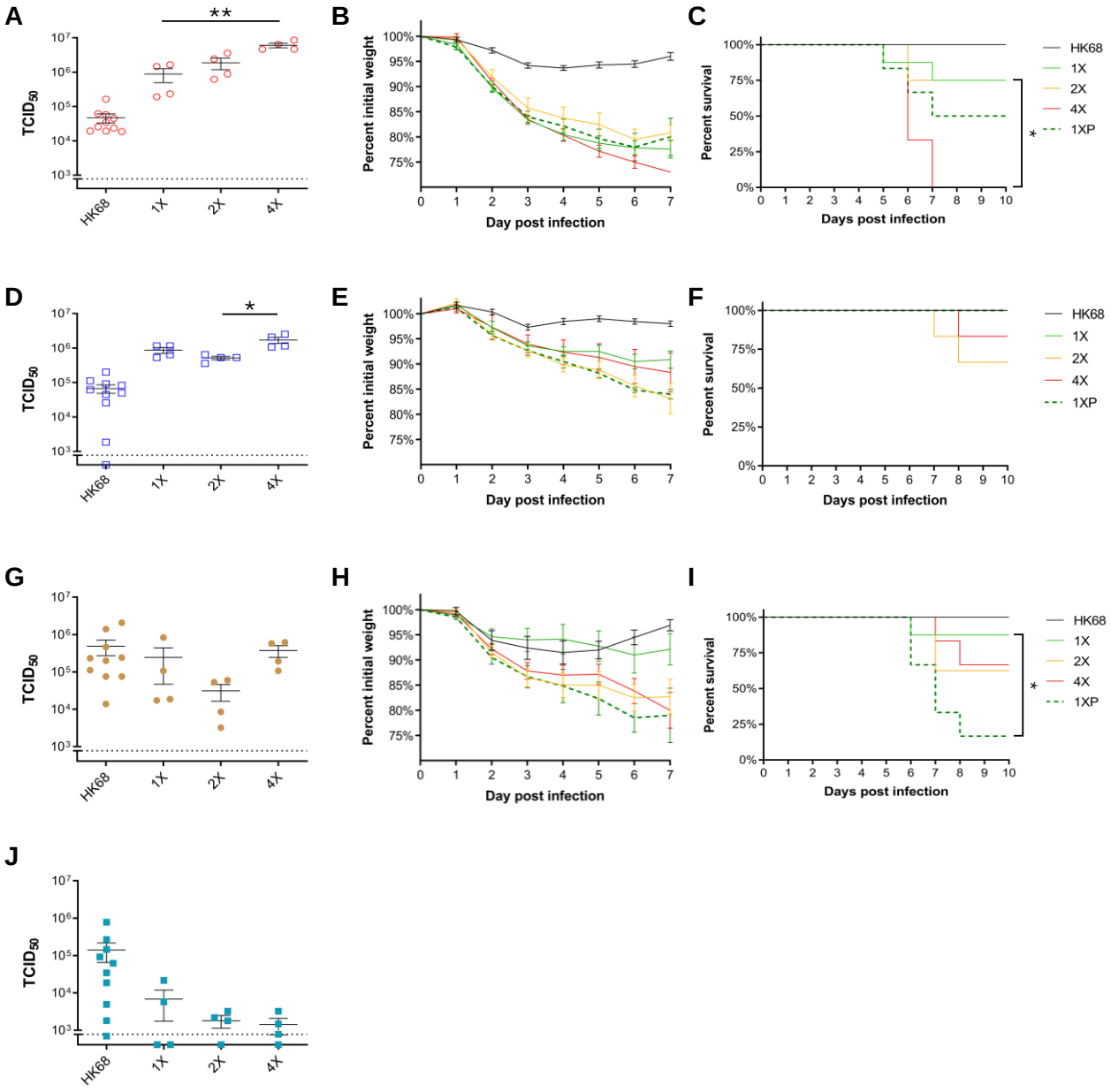

Fig. S2 – Titers (A, D, G, J), weight loss (B, E, H) and survival (C, F, I) for the different passage treatments (1X - green, 2X - gold, 4X - red) and the single multiple infection event (1XP – dashed dark green), separated by host (BALBF: A–C, BALBM: D–F, BL6F: G–I, BALBM: J)

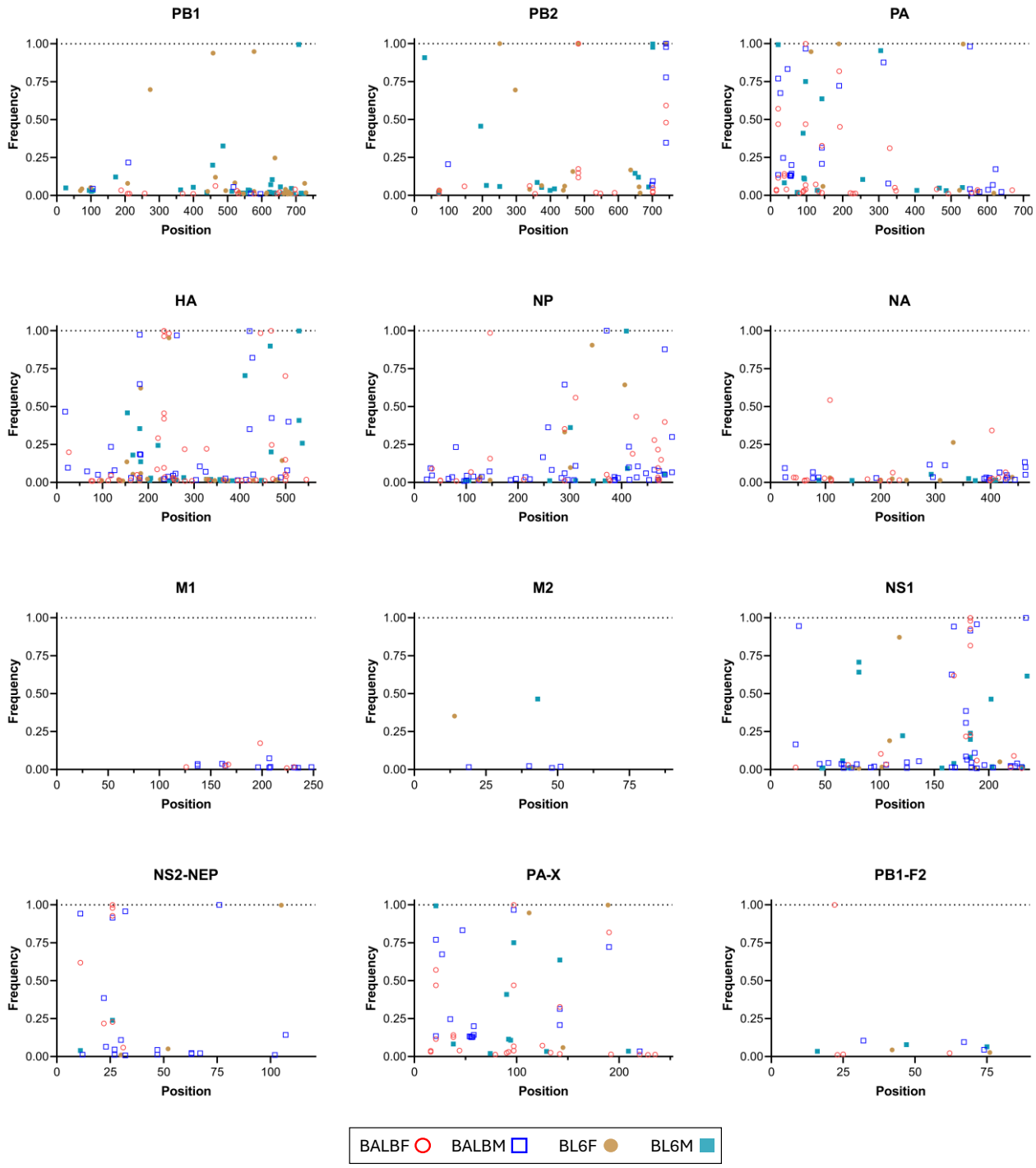

Fig. S3 – Variant frequency maps for the 12 main influenza open reading frames. Variants are from 28 independent viral lineages, 7 lineages per host type.

A

Measure	BALBF	BALBM	BL6F	BL6M	KW statistic	p value
Mean number of deletions	3	4.2	5.43	8.29	**40.53**	**<0.001**
Mean length of deletions	7.25	14.71	19.16	22.22	**11.23**	**0.011**
Mean frequency of deletions	0.098	0.080	0.076	0.083	3.77	0.287

B

Measure	BALB/c	C57BL/6	W statistic	p value
Mean number of deletions	3.67	6.86	**414.5**	**<0.001**
Mean length of deletions	12	21.01	**1156.5**	**0.021**
Mean frequency of deletions	0.087	0.08	1682	0.599

C

Measure	F	M	W statistic	p value
Mean number of deletions	4.55	6.58	2099.5	0.547
Mean length of deletions	16.3	20.23	**1524**	**0.029**
Mean frequency of deletions	0.081	0.083	1894	0.697

Table S2 – Deletion measurements and statistics. A) Comparisons between host types. B) Comparison between host strains. C) Comparisons between host sexes.

BIBLIOGRAPHY

1. Thakur, V., Bhola, S., Thakur, P., Patel, S.K.S., Kulshrestha, S., Ratho, R.K., and Kumar, P. (2022). Waves and variants of SARS-CoV-2: understanding the causes and effect of the COVID-19 catastrophe. Infection *50*, 309–325. https://doi.org/10.1007/s15010-021-01734-2.

2. Markov, P.V., Ghafari, M., Beer, M., Lythgoe, K., Simmonds, P., Stilianakis, N.I., and Katzourakis, A. (2023). The evolution of SARS-CoV-2. Nat Rev Microbiol *21*, 361–379. https://doi.org/10.1038/s41579-023-00878-2.

3. Taylor, A.L., and Starr, T.N. (2023). Deep mutational scans of XBB.1.5 and BQ.1.1 reveal ongoing epistatic drift during SARS-CoV-2 evolution. PLoS Pathog *19*, e1011901. https://doi.org/10.1371/journal.ppat.1011901.

4. Trammell, R.A., Liberati, T.A., and Toth, L.A. (2012). Host genetic background and the innate inflammatory response of lung to influenza virus. Microbes and Infection *14*, 50–58. https://doi.org/10.1016/j.micinf.2011.08.008.

5. Horby, P., Nguyen, N.Y., Dunstan, S.J., and Baillie, J.K. (2012). The Role of Host Genetics in Susceptibility to Influenza: A Systematic Review. PLoS ONE *7*, e33180. https://doi.org/10.1371/journal.pone.0033180.

6. Klein, S.L., and Flanagan, K.L. (2016). Sex differences in immune responses. Nat Rev Immunol *16*, 626–638. https://doi.org/10.1038/nri.2016.90.

7. Takahashi, T., and Iwasaki, A. (2021). Sex differences in immune responses. Science *371*, 347–348. https://doi.org/10.1126/science.abe7199.

8. Cousineau, S.V., and Alizon, S. (2014). Parasite evolution in response to sex-based host heterogeneity in resistance and tolerance. J of Evolutionary Biology *27*, 2753–2766. https://doi.org/10.1111/jeb.12541.

9. Turner, P.E., and Elena, S.F. (2000). Cost of Host Radiation in an RNA Virus. Genetics *156*, 1465–1470. https://doi.org/10.1093/genetics/156.4.1465.

10. Kubinak, J.L., Ruff, J.S., Hyzer, C.W., Slev, P.R., and Potts, W.K. (2012). Experimental viral evolution to specific host MHC genotypes reveals fitness and virulence trade-offs in alternative MHC types. Proc. Natl. Acad. Sci. U.S.A. *109*, 3422–3427. https://doi.org/10.1073/pnas.1112633109.

11. Kubinak, J.L., and Potts, W.K. (2013). Host resistance influences patterns of experimental viral adaptation and virulence evolution. Virulence *4*, 410–418. https://doi.org/10.4161/viru.24724.

12. McClelland, E.E., Adler, F.R., Granger, D.L., and Potts, W.K. (2004). Major histocompatibility complex controls the trajectory but not host-specific adaptation

during virulence evolution of the pathogenic fungus *Cryptococcus neoformans*. Proc. R. Soc. Lond. B *271*, 1557–1564. https://doi.org/10.1098/rspb.2004.2736.

13. Prokopyeva, E.A., Sobolev, I.A., Prokopyev, M.V., and Shestopalov, A.M. (2016). Adaptation of influenza A(H1N1)pdm09 virus in experimental mouse models. Infection, Genetics and Evolution *39*, 265–271. https://doi.org/10.1016/j.meegid.2016.01.022.

14. Duneau, D., and Ebert, D. (2012). Host Sexual Dimorphism and Parasite Adaptation. PLoS Biol *10*, e1001271. https://doi.org/10.1371/journal.pbio.1001271.

15. Duneau, D., Luijckx, P., Ruder, L.F., and Ebert, D. (2012). Sex-specific effects of a parasite evolving in a female-biased host population. BMC Biol *10*, 104. https://doi.org/10.1186/1741-7007-10-104.

16. Lee, S.-A., Kim, K.-J., Kim, D.-W., and Kim, B.-J. (2013). Male-Specific W4P/R Mutation in the Pre-S1 Region of Hepatitis B Virus, Increasing the Risk of Progression of Liver Diseases in Chronic Patients. J Clin Microbiol *51*, 3928–3936. https://doi.org/10.1128/JCM.01505-13.

17. Vom Steeg, L.G., and Klein, S.L. (2016). SeXX Matters in Infectious Disease Pathogenesis. PLoS Pathog *12*, e1005374. https://doi.org/10.1371/journal.ppat.1005374.

18. Farci, P., Strazzera, R., Alter, H.J., Farci, S., Degioannis, D., Coiana, A., Peddis, G., Usai, F., Serra, G., Chessa, L., et al. (2002). Early changes in hepatitis C viral quasispecies during interferon therapy predict the therapeutic outcome. Proc. Natl. Acad. Sci. U.S.A. *99*, 3081–3086. https://doi.org/10.1073/pnas.052712599.

19. Honce, R., Karlsson, E.A., Wohlgemuth, N., Estrada, L.D., Meliopoulos, V.A., Yao, J., and Schultz-Cherry, S. (2020). Obesity-Related Microenvironment Promotes Emergence of Virulent Influenza Virus Strains. mBio *11*, e03341-19. https://doi.org/10.1128/mBio.03341-19.

20. McCrone, J.T., Woods, R.J., Martin, E.T., Malosh, R.E., Monto, A.S., and Lauring, A.S. (2018). Stochastic processes constrain the within and between host evolution of influenza virus. eLife *7*, e35962. https://doi.org/10.7554/eLife.35962.

21. Xue, K.S., and Bloom, J.D. (2020). Linking influenza virus evolution within and between human hosts. Virus Evolution *6*, veaa010. https://doi.org/10.1093/ve/veaa010.

22. Vignuzzi, M., Stone, J.K., Arnold, J.J., Cameron, C.E., and Andino, R. (2006). Quasispecies diversity determines pathogenesis through cooperative interactions in a viral population. Nature *439*, 344–348. https://doi.org/10.1038/nature04388.

23. Martin, B.E., and Brooke, C.B. (2019). Flu Shows the Power of Diversity. Cell *176*, 9–10. https://doi.org/10.1016/j.cell.2018.12.017.

24. Vahey, M.D., and Fletcher, D.A. (2019). Low-Fidelity Assembly of Influenza A Virus Promotes Escape from Host Cells. Cell *176*, 281-294.e19. https://doi.org/10.1016/j.cell.2018.10.056.

25. Potter, B.I., Kondor, R., Hadfield, J., Huddleston, J., Barnes, J., Rowe, T., Guo, L., Xu, X., Neher, R.A., Bedford, T., et al. (2019). Evolution and rapid spread of a reassortant A(H3N2) virus that predominated the 2017–2018 influenza season. Virus Evolution *5*, vez046. https://doi.org/10.1093/ve/vez046.

26. Ghedin, E., Fitch, A., Boyne, A., Griesemer, S., DePasse, J., Bera, J., Zhang, X., Halpin, R.A., Smit, M., Jennings, L., et al. (2009). Mixed Infection and the Genesis of Influenza Virus Diversity. J Virol *83*, 8832–8841. https://doi.org/10.1128/JVI.00773-09.

27. Maljkovic Berry, I., Melendrez, M.C., Li, T., Hawksworth, A.W., Brice, G.T., Blair, P.J., Halsey, E.S., Williams, M., Fernandez, S., Yoon, I.-K., et al. (2016). Frequency of influenza H3N2 intra-subtype reassortment: attributes and implications of reassortant spread. BMC Biol *14*, 117. https://doi.org/10.1186/s12915-016-0337-3.

28. Liu, W., Li, Z., Tang, F., Wei, M., Tong, Y., Zhang, L., Xin, Z., Ma, M., Zhang, X., Liu, L., et al. (2010). Mixed Infections of Pandemic H1N1 and Seasonal H3N2 Viruses in 1 Outbreak. CLIN INFECT DIS *50*, 1359–1365. https://doi.org/10.1086/652143.

29. Pillai, T.K., Johnson, K.E., Song, T., Gregianini, T.S., Tatiana G., B., Wang, G., Medina, R.A., Van Bakel, H., García-Sastre, A., Nelson, M.I., et al. (2023). Tracking the emergence of antigenic variants in influenza A virus epidemics in Brazil. Virus Evolution *9*, vead027. https://doi.org/10.1093/ve/vead027.

30. Alizon, S., De Roode, J.C., and Michalakis, Y. (2013). Multiple infections and the evolution of virulence. Ecology Letters *16*, 556–567. https://doi.org/10.1111/ele.12076.

31. Bose, J., Kloesener, M.H., and Schulte, R.D. (2016). Multiple-genotype infections and their complex effect on virulence. Zoology *119*, 339–349. https://doi.org/10.1016/j.zool.2016.06.003.

32. Curtis, K. (2020). The Effect of Inflammatory Components on Influenza A Virulence Evolution.

33. Brown, E.G., Liu, H., Kit, L.C., Baird, S., and Nesrallah, M. (2001). Pattern of mutation in the genome of influenza A virus on adaptation to increased virulence in the mouse lung: Identification of functional themes. Proc. Natl. Acad. Sci. U.S.A. *98*, 6883–6888. https://doi.org/10.1073/pnas.111165798.

34. Narasaraju, T., Sim, M.K., Ng, H.H., Phoon, M.C., Shanker, N., Lal, S.K., and Chow, V.T.K. (2009). Adaptation of human influenza H3N2 virus in a mouse pneumonitis model: insights into viral virulence, tissue tropism and host pathogenesis. Microbes and Infection *11*, 2–11. https://doi.org/10.1016/j.micinf.2008.09.013.

35. Ping, J., Dankar, S.K., Forbes, N.E., Keleta, L., Zhou, Y., Tyler, S., and Brown, E.G. (2010). PB2 and Hemagglutinin Mutations Are Major Determinants of Host Range and Virulence in Mouse-Adapted Influenza A Virus. J Virol *84*, 10606–10618. https://doi.org/10.1128/JVI.01187-10.

36. Chu, J.T., Gu, H., Sun, W., Fan, R.L., Nicholls, J.M., Valkenburg, S.A., and Poon, L.L. (2023). Heterosubtypic immune pressure accelerates emergence of influenza A virus escape phenotypes in mice. Virus Research *323*, 198991. https://doi.org/10.1016/j.virusres.2022.198991.

37. Keleta, L., Ibricevic, A., Bovin, N.V., Brody, S.L., and Brown, E.G. (2008). Experimental Evolution of Human Influenza Virus H3 Hemagglutinin in the Mouse Lung Identifies Adaptive Regions in HA1 and HA2. J Virol *82*, 11599–11608. https://doi.org/10.1128/JVI.01393-08.

38. Hartley, C.A., Reading, P.C., Ward, A.C., and Anders, E.M. (1997). Changes in the hemagglutinin molecule of influenza type A (H3N2) virus associated with increased virulence for mice. Arch. Virol. *142*, 75–88. https://doi.org/10.1007/s007050050060.

39. Tate, M.D., Job, E.R., Brooks, A.G., and Reading, P.C. (2011). Glycosylation of the hemagglutinin modulates the sensitivity of H3N2 influenza viruses to innate proteins in airway secretions and virulence in mice. Virology *413*, 84–92. https://doi.org/10.1016/j.virol.2011.01.036.

40. Ping, J., Keleta, L., Forbes, N.E., Dankar, S., Stecho, W., Tyler, S., Zhou, Y., Babiuk, L., Weingartl, H., Halpin, R.A., et al. (2011). Genomic and Protein Structural Maps of Adaptive Evolution of Human Influenza A Virus to Increased Virulence in the Mouse. PLoS ONE *6*, e21740. https://doi.org/10.1371/journal.pone.0021740.

41. Kamal, R.P., Katz, J.M., and York, I.A. (2014). Molecular Determinants of Influenza Virus Pathogenesis in Mice. In Influenza Pathogenesis and Control - Volume I Current Topics in Microbiology and Immunology., R. W. Compans and M. B. A. Oldstone, eds. (Springer International Publishing), pp. 243–274. https://doi.org/10.1007/82_2014_388.

42. Steidle, S., Martínez-Sobrido, L., Mordstein, M., Lienenklaus, S., García-Sastre, A., Stäheli, P., and Kochs, G. (2010). Glycine 184 in Nonstructural Protein NS1 Determines the Virulence of Influenza A Virus Strain PR8 without Affecting the Host Interferon Response. J Virol *84*, 12761–12770. https://doi.org/10.1128/JVI.00701-10.

43. Ayllon, J., Russell, R.J., García-Sastre, A., and Hale, B.G. (2012). Contribution of NS1 Effector Domain Dimerization to Influenza A Virus Replication and Virulence. J Virol *86*, 13095–13098. https://doi.org/10.1128/JVI.02237-12.

44. Kerry, P.S., Ayllon, J., Taylor, M.A., Hass, C., Lewis, A., García-Sastre, A., Randall, R.E., Hale, B.G., and Russell, R.J. (2011). A Transient Homotypic Interaction Model

for the Influenza A Virus NS1 Protein Effector Domain. PLoS ONE *6*, e17946. https://doi.org/10.1371/journal.pone.0017946.

45. Aramini, J.M., Ma, L.-C., Zhou, L., Schauder, C.M., Hamilton, K., Amer, B.R., Mack, T.R., Lee, H.-W., Ciccosanti, C.T., Zhao, L., et al. (2011). Dimer Interface of the Effector Domain of Non-structural Protein 1 from Influenza A Virus. Journal of Biological Chemistry *286*, 26050–26060. https://doi.org/10.1074/jbc.M111.248765.

46. Omoto, S., Speranzini, V., Hashimoto, T., Noshi, T., Yamaguchi, H., Kawai, M., Kawaguchi, K., Uehara, T., Shishido, T., Naito, A., et al. (2018). Characterization of influenza virus variants induced by treatment with the endonuclease inhibitor baloxavir marboxil. Sci Rep *8*, 9633. https://doi.org/10.1038/s41598-018-27890-4.

47. Henle, W., and Henle, G. (1943). Interference of Inactive Virus with the Propagation of Virus of Influenza. Science *98*, 87–89. https://doi.org/10.1126/science.98.2534.87.b.

48. Chambers, L.A., and Henle, W. (1943). STUDIES ON THE NATURE OF THE VIRUS OF INFLUENZA. Journal of Experimental Medicine *77*, 251–264. https://doi.org/10.1084/jem.77.3.251.

49. von Magnus, P., and Gard, S. (1947). Studies on Interference in Experimental Influenza. II. Purification and Centrifugation Experiments. Arkiv for Kemi, Mineralogi och Geologi, *24 B*, 4.

50. Vignuzzi, M., and López, C.B. (2019). Defective viral genomes are key drivers of the virus–host interaction. Nat Microbiol *4*, 1075–1087. https://doi.org/10.1038/s41564-019-0465-y.

51. Alnaji, F.G., and Brooke, C.B. (2020). Influenza virus DI particles: Defective interfering or delightfully interesting? PLoS Pathog *16*, e1008436. https://doi.org/10.1371/journal.ppat.1008436.

52. Saira, K., Lin, X., DePasse, J.V., Halpin, R., Twaddle, A., Stockwell, T., Angus, B., Cozzi-Lepri, A., Delfino, M., Dugan, V., et al. (2013). Sequence Analysis of *In Vivo* Defective Interfering-Like RNA of Influenza A H1N1 Pandemic Virus. J Virol *87*, 8064–8074. https://doi.org/10.1128/JVI.00240-13.

53. Vasilijevic, J., Zamarreño, N., Oliveros, J.C., Rodriguez-Frandsen, A., Gómez, G., Rodriguez, G., Pérez-Ruiz, M., Rey, S., Barba, I., Pozo, F., et al. (2017). Reduced accumulation of defective viral genomes contributes to severe outcome in influenza virus infected patients. PLoS Pathog *13*, e1006650. https://doi.org/10.1371/journal.ppat.1006650.

54. Genoyer, E., and López, C.B. (2019). The Impact of Defective Viruses on Infection and Immunity. Annu. Rev. Virol. *6*, 547–566. https://doi.org/10.1146/annurev-virology-092818-015652.

55. Alnaji, F.G., Holmes, J.R., Rendon, G., Vera, J.C., Fields, C.J., Martin, B.E., and Brooke, C.B. (2019). Sequencing Framework for the Sensitive Detection and Precise Mapping of Defective Interfering Particle-Associated Deletions across Influenza A and B Viruses. J Virol *93*, e00354-19. https://doi.org/10.1128/JVI.00354-19.

56. Kubinak, J.L., Cornwall, D.H., Hasenkrug, K.J., Adler, F.R., and Potts, W.K. (2015). Serial infection of diverse host (*Mus*) genotypes rapidly impedes pathogen fitness and virulence. Proc. R. Soc. B. *282*, 20141568. https://doi.org/10.1098/rspb.2014.1568.

57. Cornwall, D.H., Kubinak, J.L., Zachary, E., Stark, D.L., Seipel, D., and Potts, W.K. (2018). Experimental manipulation of population-level MHC diversity controls pathogen virulence evolution in *Mus musculus*. J of Evolutionary Biology *31*, 314–322. https://doi.org/10.1111/jeb.13225.

58. Glusman, G., Rose, P.W., Prlić, A., Dougherty, J., Duarte, J.M., Hoffman, A.S., Barton, G.J., Bendixen, E., Bergquist, T., Bock, C., et al. (2017). Mapping genetic variations to three-dimensional protein structures to enhance variant interpretation: a proposed framework. Genome Med *9*, 113. https://doi.org/10.1186/s13073-017-0509-y.

59. Tichkule, S., Myung, Y., Naung, M.T., Ansell, B.R.E., Guy, A.J., Srivastava, N., Mehra, S., Cacciò, S.M., Mueller, I., Barry, A.E., et al. (2022). VIVID: A Web Application for Variant Interpretation and Visualization in Multi-dimensional Analyses. Molecular Biology and Evolution *39*, msac196. https://doi.org/10.1093/molbev/msac196.

60. Guy, A.J., Irani, V., Richards, J.S., and Ramsland, P.A. (2018). BioStructMap: a Python tool for integration of protein structure and sequence-based features. Bioinformatics *34*, 3942–3944. https://doi.org/10.1093/bioinformatics/bty474.

61. Brinton, M.A. (1983). Analysis of extracellular West Nile virus particles produced by cell cultures from genetically resistant and susceptible mice indicates enhanced amplification of defective interfering particles by resistant cultures. J Virol *46*, 860–870. https://doi.org/10.1128/jvi.46.3.860-870.1983.

62. Ngunjiri, J.M., Lee, C.-W., Ali, A., and Marcus, P.I. (2012). Influenza Virus Interferon-Inducing Particle Efficiency Is Reversed in Avian and Mammalian Cells, and Enhanced in Cells Co-Infected with Defective-Interfering Particles. Journal of Interferon & Cytokine Research *32*, 280–285. https://doi.org/10.1089/jir.2011.0102.

63. Xu, J., Sun, Y., Li, Y., Ruthel, G., Weiss, S.R., Raj, A., Beiting, D., and López, C.B. (2017). Replication defective viral genomes exploit a cellular pro-survival mechanism to establish paramyxovirus persistence. Nat Commun *8*, 799. https://doi.org/10.1038/s41467-017-00909-6.

64. Martínez-Sobrido, L., and García-Sastre, A. (2010). Generation of Recombinant Influenza Virus from Plasmid DNA. JoVE, 2057. https://doi.org/10.3791/2057-v.

65. Balish, A.L., Katz, J.M., and Klimov, A.I. (2013). Influenza: Propagation, Quantification, and Storage. CP Microbiology *29*. https://doi.org/10.1002/9780471729259.mc15g01s29.

66. Reed, L.J., and Muench, H. (1938). A SIMPLE METHOD OF ESTIMATING FIFTY PER CENT ENDPOINTS12. American Journal of Epidemiology *27*, 493–497. https://doi.org/10.1093/oxfordjournals.aje.a118408.

67. Van Elden, L.J.R., Nijhuis, M., Schipper, P., Schuurman, R., and Van Loon, A.M. (2001). Simultaneous Detection of Influenza Viruses A and B Using Real-Time Quantitative PCR. J Clin Microbiol *39*, 196–200. https://doi.org/10.1128/JCM.39.1.196-200.2001.

68. Shevach, E.M. (2011). Animal Models for Infectious Diseases. CP in Immunology *93*. https://doi.org/10.1002/0471142735.im1900s93.

69. Dinno, A. (2024). dunn.test: Dunn's Test of Multiple Comparisons Using Rank Sums.

70. Bates, D., Mächler, M., Bolker, B., and Walker, S. (2015). Fitting Linear Mixed-Effects Models Using lme4. Journal of Statistical Software *67*, 1–48. https://doi.org/10.18637/jss.v067.i01.

71. R Core Team (2021). R: A Language and Environment for Statistical Computing (R Foundation for Statistical Computing).

72. Kuznetsova, A., Brockhoff, P.B., and Christensen, R.H.B. (2017). lmerTest Package: Tests in Linear Mixed Effects Models. Journal of Statistical Software *82*, 1–26. https://doi.org/10.18637/jss.v082.i13.

73. Bartoń, K. (2024). MuMIn: Multi-Model Inference.

74. Therneau, T.M. (2024). survival: Survival Analysis.

75. Pettersen, E.F., Goddard, T.D., Huang, C.C., Couch, G.S., Greenblatt, D.M., Meng, E.C., and Ferrin, T.E. (2004). UCSF Chimera—A visualization system for exploratory research and analysis. J Comput Chem *25*, 1605–1612. https://doi.org/10.1002/jcc.20084.

76. Meng, E.C., Goddard, T.D., Pettersen, E.F., Couch, G.S., Pearson, Z.J., Morris, J.H., and Ferrin, T.E. (2023). UCSF ChimeraX : Tools for structure building and analysis. Protein Science *32*, e4792. https://doi.org/10.1002/pro.4792.